Volume 1856

Workshops and summer schools

Off-Grid Technology Workshop

Sydney, Australia
24 February 2017

Editor
Fernando Alonso-Marroquin

AIP | Conference Proceedings

proceedings.aip.org

AIP | Conference Proceedings

AIP Conference Proceedings: A name your community will know and respect

40 years' experience • 100,000+ papers • 1,700+ volumes

A world-class proceedings service for all events: From workshops to the largest international conference

- Online-only proceedings
- Optional printed copies or CDs for participants
- Rapid online and print publication

Our wealth of experience and expertise will ensure an outstanding publication experience.

Publication fees which work with your budget

- **Simple online publication fees**: Completely independent of page counts, publish substantial papers at no extra cost.
- **Options for online access**: 1-year conference access or select perpetual open access for the entire community.

Flexibility in the printed medium

Choose from these options to print all papers or just a selection of articles from the conference:

Conference collection

- Printed copies containing all papers published in the online proceedings.
- For editors who want to reproduce all online papers for their participants.

Selected papers

- Printed copies containing a selection of papers chosen by the editors.
- Choose to print just the best work, avoid the cost of printing everything.

Workshops and summer schools

- Printed copies designed especially for summer schools and workshops.
- Visibility and identity for events publishing tutorials and reviews.

Get a proposal for your proceedings in 3 simple steps

Step 1.
Obtain a proceedings questionnaire by writing to us at confproc@aip.org or download from proceedings.aip.org

Step 2.
Fill in the questionnaire with details of your conference and return it to confproc@aip.org

Step 3.
We'll review the questionnaire and your requirements and write to confirm if we can offer a proposal.

AIP Publishing

ISBN 978-0-7354-1530-0
ISSN 0094-243X

proceedings.aip.org

AIP

Off-Grid Technology Workshop

Vol. 1856

Workshops and summer schools

Off-Grid Technology Workshop

Sydney, Australia
24 February 2017

Editor
Fernando Alonso-Marroquin
The University of Sydney, Sydney, Australia

Sponsoring Organization
The University of Sydney

All papers have been peer reviewed.

AIP Publishing

Melville, New York, 2017
AIP Conference Proceedings

Volume 1856

To learn more about AIP Conference Proceedings visit **http://proceedings.aip.org**

Editor

Fernando Alonso-Marroquin
The University of Sydney
J05, School of Civil Engineering
Sydney NSW 2006
Australia

Email: fernando@sydney.edu.au

ISBN 978-0-7354-1530-0
ISSN 0094-243X
Printed in the United States of America

AIP Conference Proceedings, **Volume 1856**
Off-Grid Technology Workshop

Table of Contents

Workshop on Off-grid Technology Systems

Fernando Alonso-Marroquin

School of Civil Engineering, The University of Sydney, Australia

fernando@sydney.edu.au

Abstract. Off-grid houses are dwellings that do not rely on water supply, sewer, or electrical power grid, and are able to operate independently of all public utility services. These houses are ideal for remote communities or population suffering natural or human-made disasters. Our aim is to develop compact and affordable off-grid technologies by integrating high-end nano-engineering with systems that imitates natural biological processes. The key areas of focus in the workshop were: solar energy harvesting using nanotechnology, wind energy harvesting from vertical-axis wind turbines, supercapacitors energy storage systems, treatment of greywater, and green roofs to achieve air comfort.

WORKSHOP

Here I present the papers resulting from the Workshop in Off-Grid Technology Systems organized at The University of Sydney on Friday, February 24, 2017. Our vision is to create a research community to drive new innovations in off-grid technologies. The targeted areas of our current research in the area are: solar energy harvesting, wind energy harvesting, passive cooling systems, energy storage systems, green roofs, vertical farming, treatment of rainwater, greywater, and blackwater, passive houses, modular houses, and small scale composting reactors. The workshop was an international meeting were 18 speakers from academia and industry presented their vision in four different topics: sustainable building, energy harvesting and storage, food production, and passive cooling.

CONTRIBUTIONS

The contributions presented in this volume correspond to advances in nanotechnology in the areas of solar energy harvesting and storage, and experimental and numerical research performed in Sydney with the aim to improve the technologies for off-grid sustainable housing.

Arias-Calluari and Alonso-Marroquin [1] present an overview of the off-grid house project and a numerical analysis of the structure of the off-grid modular house. Two key aspects of off-grid houses are energy harvesting and energy storage, which are active research areas. The papers of Reddy and Alonso-Marroquin [2, 3] present developments on highly efficient nanomaterials-based electrodes for high-performance batteries and high efficiency solar panels. The paper of Hallock et al [4] presents an alternative to solar panel for harvesting of wind energy using vertical axis wind turbines. The paper discusses the difficulties to achieve acceptable efficiencies using commercially available vertical axis wind turbines, and proposes methods to overcome these challenges.

In the area of water treatment, Mc Donald et al. [5] introduces a method to treat grey water using a vertical garden. This garden is an efficient integration of wet land systems, sand filter, and hydroponic system to achieve water clean enough that can be reused for irrigation of flushing.

Off-Grid Technology Workshop
AIP Conf. Proc. 1856, 010001-1–010001-2; doi: 10.1063/1.4985551
Published by AIP Publishing. 978-0-7354-1530-0/$30.00

Since the off-grid modular houses are smaller than conventional houses, they present a small thermal mass and thus are susceptible to strong temperature variations. The paper of Castiglia-Feitosa and Wilkinson [6] proposes a solution of this problem using green roof and walls, which significantly reduces the temperature but at the same time they increase the humidity. Their paper proposed an algorithm for calculation of heat index. Their experimental results shows that green roof and walls significantly improve the air conform inside the house.

The paper of Alonso-Marroquin et al [7] presents the implementation of a stand-alone solar energy system for the off-grid house using commercial available components. It is shown that solar panel a moderate amount of power to cover the main necessities of the house occupants.

CONCLUSIONS

We have successfully built a prototype of off-grid house that operates with solar energy harvesting, wind energy harvesting, energy storage, and grey water treatment. One of the key issues that has not been addressed at the moment is the off-grid toilet, which requires a passive ways to separate urine from faeces and efficient composting methods. The energy collection is prone to inefficiencies that need to be addressed in the near future, especially by reducing of the dissipation of the wind turbine and using hybrid composite nano-materials for more efficient solar energy systems.

ACKNOWLEDGMENTS

I thank of the participants that for various reasons did not publish in this volume but contributed in the workshop: Michael Mobbs, Tony Vassallo, Brian Jones, Louis Saadeh, Kapil Chauhan, Erich Hepp, Claudia Echeverria, and Catalina Galindo. Special thanks to Coraline Chiew for taking care the logistics of the workshop.

REFERENCES

1. K. Arias Calluari and F. Alonso-Marroquin, “Structural Analysis of an Off-Grid Tiny House”, AIP Conf. Proc. 1856, 020001 (2017).
2. K. R. Reddy and F. Alonso-Marroquin, “Polypyrrole Functionalized with Carbon Nanotubes as an Efficient and New Electrodes for Electrochemical Supercapacitors”, AIP Conf. Proc. 1856, 020002 (2017).
3. K. R. Reddy and F. Alonso-Marroquin, “Graphene oxide functionalized with silver nanoparticles as conducting electrodes for solar cells and electrochemical energy storage devices”, AIP Conf. Proc. 1856, 020003 (2017).
4. K. Hallock, T. Rasch, G. Ju, and F. Alonso-Marroquin, “Efficiency of the DOMUS 750 Vertical-Axis Wind Turbine”, AIP Conf. Proc. 1856, 020004 (2017).
5. A. P. McDonald, A. Montoya, and F. Alonso-Marroquin, “Vertical Garden for Treating Greywater”, AIP Conf. Proc. 1856, 020005 (2017).
6. R. Castiglia Feitosa and S. Wilkinson, “Retrofitted Green Roofs and Walls and Improvements in Thermal Comfort”, AIP Conf. Proc. 1856, 020006 (2017).
7. F. Alonso-Marroquin, J. B. Gormly, and J. Bilbao, “Stand Alone Solar Energy Harvesting and Storage Systems in Off-Grid Applications”, AIP Conf. Proc. 1856, 020007 (2017).

Structural Analysis of an Off-Grid Tiny House

Karina Arias Calluari[1,a)] and Fernando Alonso-Marroquín[1,b)]

[1)] *School of Civil Engineering, The University of Sydney, Australia*

Corresponding authors: [a)] kari0293@sydney.edu.au [b)]fernando@sydney.edu.au

Abstract.
The off-grid technologies and tiny house movement have experimented an unprecedented growth in recent years. Putting both sides together, we are trying to achieve an economic and environmental friendly solution to the higher cost of residential properties. This solution is the construction of off-grid tiny houses. This article presents a design for a small modular off-grid house made by pine timber. A numerical analysis of the proposed tiny house was performed to ensure its structural stability. The results were compared with the suggested serviceability limit state criteria, which are contended in the Australia Guidelines Standards making this design reliable for construction.

1. INTRODUCTION

At this time, the sustainable and reusable design are playing important roles in human activities due to environmental impacts [1]. Electricity supplies and construction are biggest issues as a consequence of the embodied energy and greenhouse gases involved [2]. In USA the energy consumption in 2016 was 39.5% due to residential and commercial buildings sectors [3], considering their total energy consumption until November 2016 [4].

Australia energy consumption is not far away from this fact. The previous statistics of 2016 showed that construction and electricity supplies have an average annual growth of 2.0% and 5.5% respectively of energy consumption [2]. However, off grid technologies played an important role to make this percentage decrease from 2008 to 2009 [2], although it seems to be not enough to diminish annual growth. For that specific reason an improvement of the conservation with renewable energy must be established.

Some authors were focused particularly on off grid homes as part of energy conservation' solution [5-7]. And the most attractive part is the final price that you can achieve having an off grid home [7].

On the other hand, Australian bureau statistics show that residential property has had a sustained increase of prices. Sydney has the highest rate of increase, getting 2.6% in September 2016 quarter [8], being the mean price of an apartment $631 000 AUD [9]. This information seems to be the reason of falling -3.3% in new residential building activity [10], because it is unaffordable for people. It is important to clarify that vacant residential land is not included in the value of dwelling stocks [11]. Nevertheless, Australian vacant land has experimented an upward trend. The median vacant land price in Australia until March 2016 quarter was $235 000 AUD [12].

The off-grid homes as part of solution of reusable energy and the uptrend of land and construction prices, both of them give the idea that off-grid tiny houses could be a good solution. Many authors confirm that off-grid homes are the best solutions for energy conservation because you would be able to ensure your own home with a cost-effective result [7, 13]. As stated by Murphy (2014), it is possible to construct your own tiny and environmentally friendly house with only $5000.00 American dollars [7]. Murphy (2014) refers in her article to

Off-Grid Technology Workshop
AIP Conf. Proc. 1856, 020001-1–020001-12; doi: 10.1063/1.4985552
Published by AIP Publishing. 978-0-7354-1530-0/$30.00

a house of 6.69m2 to 11.89 m2— fitting in footprint of trailers — governed by shipping containers and RV's laws in the United States**.**

Nonetheless, during this research it was noticeable the lack of information about proper off-grid tiny house and how to construct them, because most of them are related to houses with hybrid systems [13-15] and energy consumption analysis [6, 16]. Consequently, this paper proposes a model to analyse the architecture and structural analysis considering all the necessities that a standard citizen could have. The architectural design was carried out using Sketch Up Pro 2015 and Architectural Revit 2017. The Structural analysis was executed with ETABS V.9.2. For that purpose were considered Clayton, Warden (2002) and Sareh's (2014) comments of 3D modelling and computer simulation [1, 17]. The proper construction of the off grid tiny house —taking out the equipment — should fit in an investment of $ 6 200 AUD. It is important to clarify that this amount corresponds to a basic off-grid tiny house model and this will vary depending on the level of the design that dwellers put into their tiny homes.

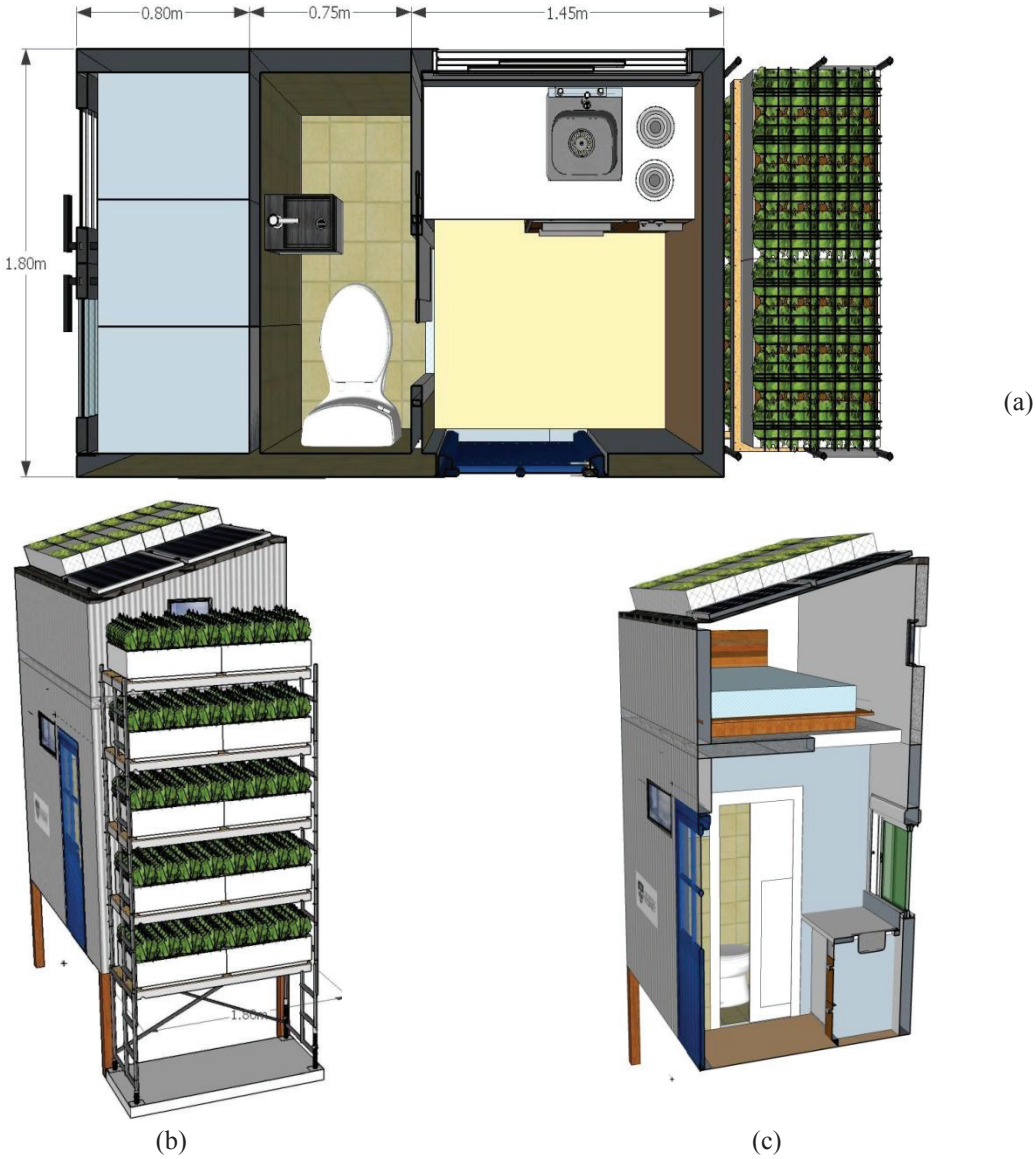

FIGURE 1. (a) Horizontal view of the proposed 3D model (first level) (b) Outside view of the proposed 3D architectural model of the off-grid tiny house. (c) Inside view of the proposed 3D architectural model of the off-grid tiny house.

There are strong reasons to be focus on developing this 3-D model. It has been stated that virtual construction could be considered as an instrumental technique of estimating cost as a result of a pre-integration of different specialties and drafting construction [17]. Thus, the owners, builders and any stakeholder's ideas could be easily considered. Moreover, one of the characteristics that enhance 3D models by Clayton, Warden (2002) is that people with minor practical knowledge of construction methods and management experience could compensate their low expertise and contribute heavily during the construction process [17]. Also, Murphy (2014) affirms that blueprints are not enough to catch the purpose and offer the facilities to a common dweller to construct it by themselves making the 3D virtual model the best option to control this issue[7]. Murphy (2014) indicates that even if the tiny-house owners obtain they purchased blueprints, they customize the interior of their own homes because they want them to be different. In consequence, they could increase abruptly the price or, if the worst comes to the worst, they would make it environmentally less friendly from what it was planned.

1.1 Description of Off-Grid Tiny House Model

The purpose of this tiny house is to be an off grid unit, with its own recycling system of rainwater and graywater through a filter sand systems [18] to be capable to cover the main necessity of humans "drinking water" ensuring a good water quality [19]. In the case of energy, this will be provided by the sun and wind velocity. This energy will be stored in batteries for continuous use. *Fig.1* shows the proposed tiny off-grid house.

Because of that, special considerations during the design of the tiny house were made. First, the ground floor of the tiny house must be an empty space, this will contain two tanks one for grey water and the other for clean water storage. This design was made in base on the compendium of Sanitation Systems and Technologies templates [20]. In which the clean water tank will store the stormwater and the grey water tank will store water from bathing and washing that may content traces of excreta and small quantity of pathogens. These systems require to design the columns and beam structural frame in such a way that it will allow enough empty space for the storage of these tanks and the pipes connections. The frame is shown in *Fig.2*. The frame and the walls should be designed to withstand stresses, especially those caused by the wind forces and loads over the roof.

A green roof is proposed for this tiny house. The purposes of this roof are twofold: energy collection and air comfort. For energy collection, there will be PV panels on the roof properly that should be oriented to optimize the solar collection [21]. Therefore, the roof must be a free space with an elevation angle of 15°, which is the complementary of the elevation angle of the Sun in summer in Sydney. The air comfort will be improved by placing a vegetation at the roof [22]. The green roof is made up of a set of drawers. The drawers will contain plants and soil, which will help to maintain a constant temperature inside the house. In few words these tiny home has a passive solar and cooling design strategy allowing a significant reductions in energy consumption because it only uses ambient energy sources [23-25].

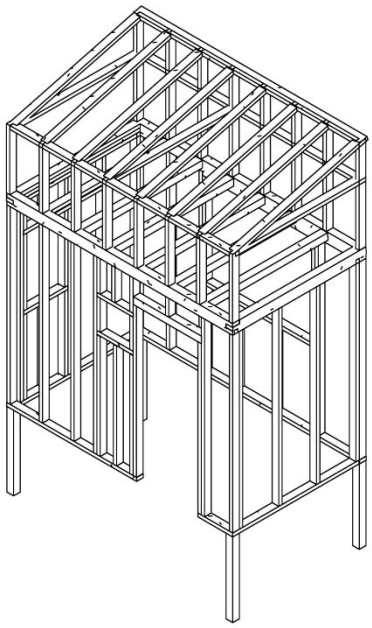

FIGURE 2 3D model of a simple column & beam structural system. The main material is of pine wood.

A small bathroom and a kitchen are proposed in the first floor of the house. In the second floor we propose a bunk bed. These will cover the necessary space for a comfortable life style in the house. The toilet will have an off-grid system. Flush water will be supplied from treated grey water from the sink, bath, and

kitchen. An Aquatron, — a Swedish wet composting system [26] — is proposed to solid-liquid separation of the toilet outlet, and the sewage sludge will be disposed in a composting system and a wetland system.

A sound level of thermal insulation in the house will be provided to this construction, considering that this tiny house will ensure a person to live well and enjoy the right temperature variation for a correct operation of the batteries and systems that will be contended inside.

The main construction material is pine wood for the frame and plywood for the walls. The choice of pine is motivated by its availability at low price, lowest carbon footprint, and low orthotropic properties compared with other woods [27] and easiness to be obtained by dwellers.

All the characteristics in conjunction of this tiny off grid house make this design a sustainable one. 'Maximizing the quality of building environment and minimizing or eliminating the negative effects' [28].

2. 3-D MODEL

2.1 Structural Model

The structure analysed in this project is proposed to be made from pine wood as the main material. The procedure for determining the structural analysis and the final structural design of the presented Off-Grid Tiny house follows the next steps guided by AS/NZS 1170.0:2002 [29]

(a) Determine the actions –permanent, imposed and others– and the loads as consequence of them following AS/NZS 1170.1:2002 [30].
(b) Determine wind pressure over the house and their consequence AS/NZS 1170.2:2011[31].
(c) Calculate earthquake actions over the off grid Tiny house AS 1170.4-2007[32]
(d) Calculate the combinations of actions for ultimate limit states —stability and strength— and serviceability AS/NZS 1170.0:2002 [29]. The properties of the pine wood — main material— was taken from Green David & Winandy, Jerrold E. research [33]

2.1.1 Structural design actions (G) & (Q)

Dead Load (G): The house is made by pine wood, The density of pine is 380 kg/m^3 [33], given in total mass of approximately 2 tonnes for the frame proposed considering walls and floors.
Live Load (Q): Considering Australia/New Zeland Standard AS/NZS 1170.1:2002 [30] for this house (Category C) 1.5 kPa is considered as uniformly distributed action.

2.1.2 Wind pressure (W):

For wind loads, AS/NZS 1170.2:2011 [31] was applied. We consider the following parameters:
- The off grid tiny house has one shed roof with a slope $\alpha = 14^{\circ}$ and an average roof height $h = 4.524m$
- The location is in Australia Sydney with a Terrain Category Nr. 2.
- Number of meters above sea level is —worst case scenario—200 m approximately for Sydney [34].
- Different wind directions are considered therefore to be a mobile house.

Applying the considerations described above, the following results were obtained from the analysis. The results are shown in *Table 1*.

$$p = (0.5\rho_{air})\left[V_{des,\theta}\right]^2 C_{dyn} C_{fig} \qquad (1)$$

TABLE 1: Parameters to obtain the wind pressure

$\rho_{air} = 1.2kg/m^3$		Density of air
$V_{des,\theta} = 43.13m/s$		Design wind speed, (maximum value of $V_{sit,\beta}$).
$V_{sit,\beta} = 43.13m/s$		Site wind speed. Annual exceedance probability of 1/100 in AU
$C_{dyn} = 1$		Dynamic response factor.
C_{fig} (*)	$C_{fig,i} = -0.27$	Aerodynamic shape factor internal
	$C_{fig,e,w} = 0.72$	Aerodynamic shape factor external for windward walls
	$C_{fig,e,l} = -0.27$	Aerodynamic shape factor external for leeward walls
	$C_{fig,e,s} = -0.585$	Aerodynamic shape factor external for side walls
	$C_{fig,e,u} = -0.675$	Aerodynamic shape factor external for upwind roof
	$C_{fig,e,d} = -0.45$	Aerodynamic shape factor external for downwind roof
	$C_{fig,e,r} = -0.54$	Aerodynamic shape factor external for crosswind roof

(*)Note: C_{fig} is the Aerodynamic shape factor. Depends on pressure direction, as a consequence has different values over the walls and roof analysed.

TABLE 2: Internal and external pressure acting on the walls and roof

$p_i = -0.30kPa$	Design internal pressure of the house
$p_{e,w} = +0.80kPa$	Design external pressure for windward walls.
$p_{e,l} = -0.30kPa$	Design external pressure for leeward walls
$p_{e,s} = -0.65kPa$	Design external pressure for side walls
$p_{e,u} = -0.75kPa$	Design external pressure for upwind roof slope
$p_{e,d} = -0.50kPa$	Design external pressure for downwind roof slope
$p_{e,r} = -0.60kPa$	Design external pressure for crosswind roof slope

Following the AS/NZS 1170.2:2011standards [31] we obtain internal and external pressures with the equation already described. The results are shown in Table 2 and a sketch of them can be observed in Fig.3, these were obtained using the corresponding C_{fig} factor.

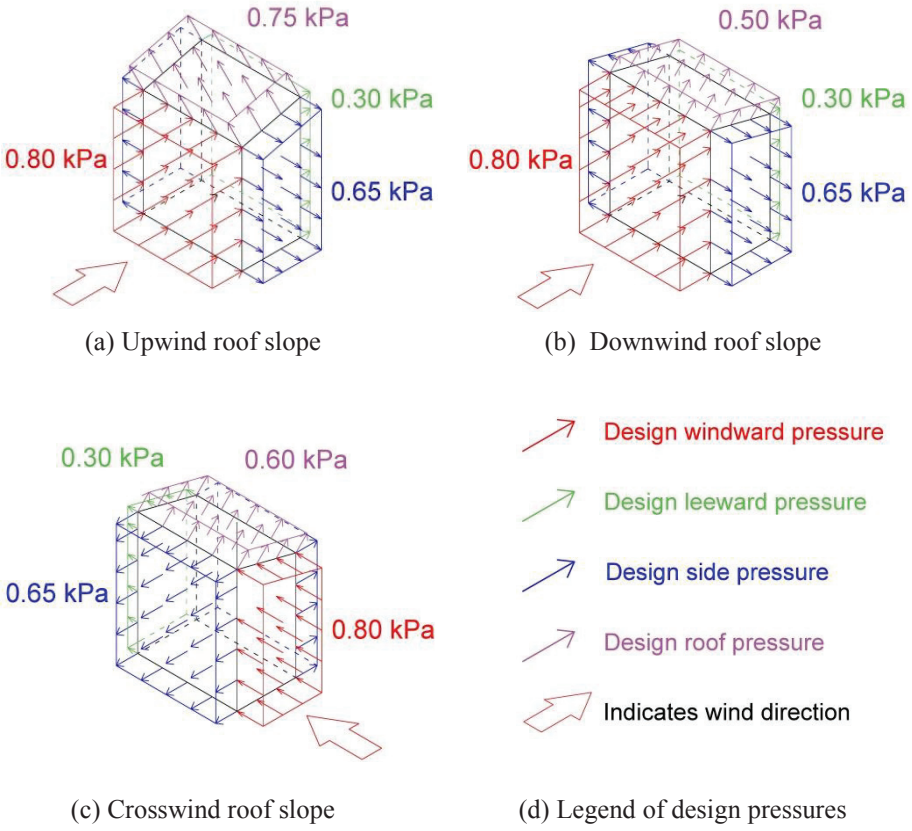

(a) Upwind roof slope (b) Downwind roof slope

(c) Crosswind roof slope (d) Legend of design pressures

FIGURE 3: Pressure for windward, leeward and side walls & upwind, downwind and crosswind for the roof for different cases which depend wind direction.

2.1.3 Earthquake Analysis (E)

For the Earthquake analysis, an equivalent static analysis was made considering that Design Category is I. The results obtained during this analysis were validated with the ones obtained in ETABS software at the moment of input the initial parameters of the off-grid house. The horizontal equivalent force V was determined by the following equation provided by AS 1170.4-2007 [32]:

$$V = C_d(T_1)W_t \qquad (2)$$

$$V = 9.316kN$$

$C_d(T_1) = 0.112$ Horizontal design action coefficient which depends of T_1.

$T_1 = 0.194seg$ The fundamental natural period.

$W_t = 83.179kN$ Total Seismic weight of the structure, for each level $W_i = \sum G_i + \sum 0.3Q_i$

Then, a vertical distribution of horizontal forces F for each level was made base on:

$$F_i = k_{F,i}V \qquad (3)$$

Where i varies from 1 to 3 corresponding to the number of floors. The $k_{F,i}$ where obtained considering the weights of the structure of each floor W_i , and the height of level h_i of each floor. The results are shown in *Fig.4.*

$F_1 = 1.412kN$ Force for the 1st level, $k_{F,1} = 0.152$ as the seismic distribution factor.

$F_2 = 4.801kN$ Force for the 2nd level, $k_{F,2} = 0.516$ as the seismic distribution factor

$F_3 = 3.097kN$ Force for the 2nd level, $k_{F,3} = 0.333$ as the seismic distribution factor

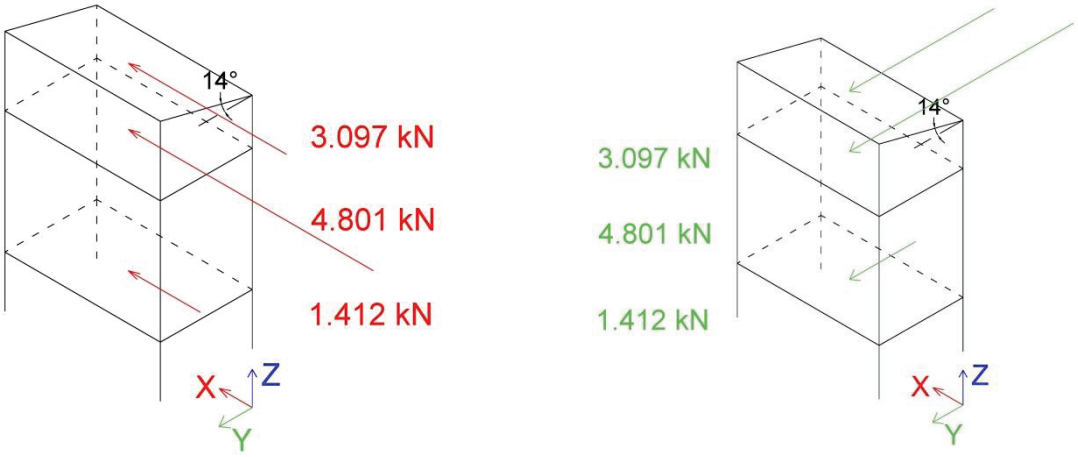

(a) Earthquake in X global direction (b) Earthquake in Y global direction

FIGURE 4: Vertical distribution of horizontal forces

2.1.4 Combinations of actions

The following combinations of load in *Table 3* were considered for the analysis, with AS/NZS 1170.0:2002 standard [29] as follows.

TABLE 3: Combinations of Loads

Stability	Strength
$0.9G$	$1.35G$
$1.35G$	$1.2G+1.5Q$
$1.2G+1.5Q$	$1.2G+1.5\psi_l Q$
$1.2G+W+\psi_c Q$	$1.2G+W+\psi_c Q$
$G+E+\psi_E Q$	$0.9G+W$
	$G+E+\psi_E Q$

$\psi_l = 0.4$ Long-term factor for residential and domestic use

$\psi_c = 0.4$ Combination factor for residential and domestic use

$\psi_E = 0.3$ Earthquake Combination factor for residential and domestic use

2.1.5 The Structural Analysis –ETABS

The Structural Analysis was made in ETABS V.9.2. The structural model was elaborated considered the architectural distribution and distances —architectural model—previously developed. The main material for the considered analysis were pine timber woods, and the information of their mechanical properties were obtained from results of previous test of small pieces of wood [33].

The modelled materials for the structural analysis are pine timbers wood with section of 90 mm × 45 mm for columns since the first level up to the roof , and section of 90 mm × 90 mm for foundation. For walls consist of shear panels of plywood (thickness of 15mm).

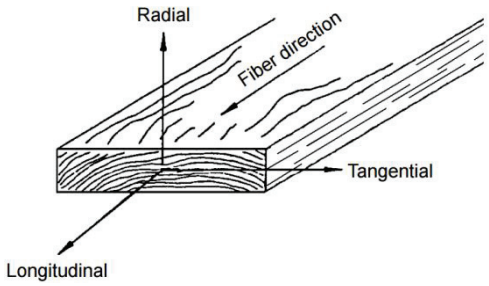

FIGURE 5: Pine timber wood axes

This pine material was modelled as an orthotropic material with the following property data shown in *Table 4*, this information was an input for ETABS V.9.2.:

TABLE 4: Mechanical properties of Pine wood [33]

Mass per unit Volume		3.73	ton/m^3
Weight per unit Volume		36.56	kN/m^3
Modulus of Elasticity	Longitudinal (1)	6900000	kN/m^2
	Tangential (2)	572700	kN/m^2
	Radial (3)	841800	kN/m^2
Poisson's Ratio	Plane (1) & (2)	0.40	
	Plane (1) & (3)	0.34	
	Plane (2) & (3)	0.39	
Coeff of Thermal Expansion	Tangential (1)	1.17(10^{-5})	
	Radial (2)	1.17(10^{-5})	
	Longitudinal (3)	1.17(10^{-5})	
Shear Modulus	Plane (1) & (2)	952200	kN/m^2
	Plane (1) & (3)	793500	kN/m^2
	Plane (2) & (3)	117300	kN/m^2

Then, all the forces, loads— G,Q, W,E — and combinations of them were applied over the model. Two types of model were proposed, the difference between them are the braces under the first floor. As it is noticeable in *Figure 6.* The results are shown in *Table 5.*

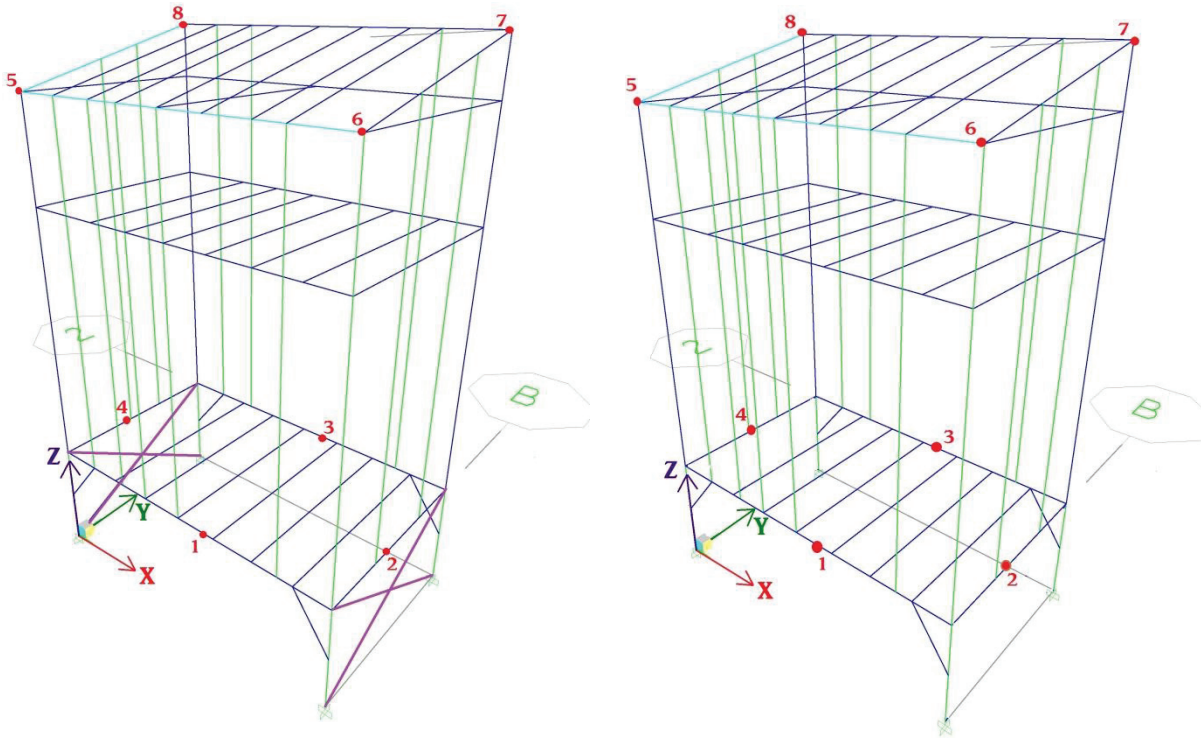

(a) Model A considering braces at the bottom

(b) Model B without braces at the bottom

FIGURE 6: Structural models evaluated with Etabs V.9.2.

TABLE 5: Results of displacement in critic points due to each different type of load and pressure over the walls, floors and roof in the house (following the legend of Fig.5).

Load		Critic point	With braces			Without braces		
			X (mm.)	Y (mm.)	Z (mm.)	X (mm.)	Y (mm.)	Z (mm.)
Dead Load (G)		1&3	+0.01	+0.05	-0.30	+0.01	+0.01	-0.50
		2&4	-0.04	-0.01	-0.30	+0.05	-0.03	-0.50
Live Load (Q)		1&3	+0.00	+0.00	-0.08	+0.00	+0.00	-0.07
		2&4	+0.00	+0.00	-0.08	+0.01	+0.01	+0.06
Wind (W)	Crosswind (+X)	2	+0.85	+0.00	+0.03	+0.84	+0.01	-0.01
		6&7	+1.03	+0.30	+0.06	+1.05	+0.02	-0.02
	Crosswind (-X)	4	-0.85	+0.00	+0.03	-0.84	+0.01	-0.01
		5&8	-1.03	+0.30	+0.06	-1.05	+0.02	-0.02
	Upwind (+Y)	3	+0.00	+0.24	-0.06	+0.00	+2.00	-0.06
		7&8	+0.00	+0.90	-0.03	-0.01	+2.65	-0.03
	Downwind (-Y)	1	+0.00	-0.30	-0.10	+0.01	-2.47	-0.10
		5&6	+0.01	-1.20	-0.09	-0.01	-3.37	-0.09
Earthquake (E)	Ex	2	+1.11	+0.00	+0.03	+1.10	-0.05	-0.03
		6&7	+1.50	-0.03	-0.04	+1.52	-0.07	-0.07
	-Ex	4	-1.11	+0.00	+0.03	-1.10	-0.05	-0.03
		5&8	-1.50	-0.03	-0.04	-1.52	-0.07	-0.07
	Ey	3	-0.01	+0.22	-0.10	+0.02	+1.77	-0.10
		7&8	+0.01	+1.11	-0.90	-0.01	+2.67	-0.09
	-Ey	1	+0.00	-0.22	-0.10	+0.00	-1.77	-0.10
		5&6	+0.02	-1.10	-0.11	+0.01	-2.61	-0.10

The overall results are obtained applying the superposition principle — adding the effects —in the worst-case scenario shown in *Table 6* and the envelope principle which considers the combinations of actions *Table 7* in each of the critic points are shown below:

TABLE 6: Comparison of the results obtained from the superposition principle in Model A and Model B

	Superposition Principle - (With braces)			Superposition Principle - (Without braces)		
	X(mm)	Y (mm)	Z (mm)	X (mm)	Y(mm)	Z(mm)
1	0.01	-0.47	-0.58	0.02	-4.23	-0.77
2	1.92	-0.01	-0.32	2.00	-0.06	-0.48
3	0.00	0.51	-0.54	0.03	3.78	-0.73
4	-2.00	-0.01	-0.32	-1.88	-0.06	-0.48
5	0.03	-2.30	-0.20	0.00	-5.98	-0.19
6	0.03	-2.30	-0.20	0.00	-5.98	-0.19
7	0.01	2.01	-0.93	-0.02	5.32	-0.12
8	0.01	2.01	-0.93	-0.02	5.32	-0.12

TABLE 7: Result from the Envelope principle with load combination in Model A and Model B

	Envelope - (With braces)			Envelope - (Without braces)		
	X(mm)	Y (mm)	Z (mm)	X (mm)	Y(mm)	Z(mm)
1	1.11	-1.30	-0.45	1.08	-2.46	-0.45
2	1.16	-0.37	-0.37	1.18	-2.45	-0.38
3	-1.11	-0.32	-0.42	-1.13	-2.50	-0.43
4	-1.15	-0.34	-0.41	-1.15	-2.52	-0.42
5	-1.47	-1.16	-0.59	-1.44	-3.35	-0.59
6	-1.46	-1.15	-0.66	-1.43	-3.33	-0.66
7	-1.53	-1.20	-0.63	-1.55	-3.38	-0.63
8	-1.52	-1.20	-0.72	-1.54	-3.39	-0.72

2.1.6 Analysis Results –ETABS

The obtained results are compared with the permissible deflections shown in AS/NZS 1170.0:2002 standards for suggested serviceability [29] as it can be observed in *Table 8*. Also, the properties of the pine wood indicated by David Wood [33] after extensive sampling and analysing procedures in the laboratory were considered.

TABLE 8: Summary of the final results of Model A and Model B with Etabs V.9.2.

			With braces			Without braces		
	`	Allowed (mm)	Method	Point	(mm)	Method	Point	(mm)
For Serviceability	Mid-Span deflection Y (Span/300-mm)	6.00	Envelope	4	-0.41	Superposition Principle	2&4	-0.48
	Mid-Span deflection X (Span/300-mm)	10.18	Superposition Principle	1	-0.58	Superposition Principle	1	-0.78
	Deflection at top (Height/200 or <12 mm)	12.00	Superposition Principle	5&6	-2.30	Superposition Principle	5&6	-5.98

3. CONCLUSION

A numerical analysis of one module of an off-grid tiny house was performed to ensure its structural stability. Two cases were analysed, the difference between them are the presence or absence of braces at the bottom. Both cases show good behaviour and deflections below the tolerance range allowable by the Australian guidelines. However, the use of braces at bottom of the tiny house will increase the stability in the tiny house, reducing the lateral displacement in approximately 4 mm at the top representing 61.5% of reduction. Two methods were used to obtain the final displacement due to the different loads: the envelope and superposition principle. The superposition principle gives higher deflection. Nevertheless, these do not reach the 50% of permitted deflections. As a conclusion, the results obtained in the previous analysis shown that this house is reliable for construction.

The structural analysis presented in this paper corresponds to the architectural design described above. The dimensions and shape of the house allows a quick and easy construction. Nevertheless, other shapes and architectural designs are under current evaluation.

4. ACKNOWLEDGMENT

Thanks to John Guoqiang Ju, Arthur McDonald, Justin Blake Gormly and Stephen Strongman, for their support and collaboration in the off-grid-house project as part of their thesis. Special thanks for Catalina Galindo-Leon for review the manuscript.

5. REFERENCES

1. Naji, S., et al., *Structure, energy and cost efficiency evaluation of three different lightweight construction systems used in low-rise residential buildings.* Energy and buildings, 2014. **84**: p. 727-739.
2. Australian Gouverment, D.o.I.I.a.S., *Australian Energy update 2016*. 2016, Australian Energy Statistics transferred to the Department of the Environment and Energy: CANBERRA ACT 2601.
3. Administration, U.S.E.I., *Energy Consumption by Sector*. 2017: Washington DC
4. Administration, U.S.E.I., *Glossary of Data Categories*. 2017.
5. Barley, C.D., P. Torcellini, and O. Van Geet. *Design and performance of the Van Geet off-grid home*. in *ASME 2003 International Solar Energy Conference*. 2003. American Society of Mechanical Engineers.
6. Barley, C.D. and P.A. Torcellini, *The van geet off-grid home: An integrated approach to energy savings*. 2004: National Renewable Energy Laboratory.
7. Murphy, M., *Tiny houses as appropriate technology.* Communities, 2014(165): p. 54.
8. Statistics, A.B.o., *6416.0 - Residential Property Price Indexes: Eight Capital Cities, Sep 2016*. 2017, Australian Bureau of Statistics: Canberra
9. Statistics, A.B.o., *Residential Dwellings: Values, Mean Price and Number by State and Territories*. 2017, ABS.Stat beta: Canberra/Australia.
10. Statistics, A.B.o., *8752.0 - Building Activity, Australia, Sep 2016*. 2016.
11. Statistics, A.B.o., *6464.0 - Residential Property Price Indexes: Concepts, Sources and Methods, 2014* 2017: Australia.
12. Logic, H.-C., *Residential Land Report*. 2016.
13. Sen, R. and S.C. Bhattacharyya, *Off-grid electricity generation with renewable energy technologies in India: An application of HOMER.* Renewable Energy, 2014. **62**: p. 388-398.
14. Fleck, B. and M. Huot, *Comparative life-cycle assessment of a small wind turbine for residential off-grid use.* Renewable Energy, 2009. **34**(12): p. 2688-2696.
15. Pradhan, S.R., et al., *Design of standalone hybrid biomass & PV system of an off-grid house in a remote area.* International Journal of Engineering Research and Application, 2013. **3**(6): p. 433-37.

16. Maher, P., N. Smith, and A. Williams, *Assessment of pico hydro as an option for off-grid electrification in Kenya.* Renewable Energy, 2003. **28**(9): p. 1357-1369.
17. Clayton, M.J., R.B. Warden, and T.W. Parker, *Virtual construction of architecture using 3D CAD and simulation.* Automation in Construction, 2002. **11**(2): p. 227-235.
18. McDonald A. P., Montoya A., and Alonso-Marroquin F., *Vertical Garden for Treating Greywater*, AIP Conf. Proc. 1856, 020005 (2017).
19. Gadgil, A., *Drinking water in developing countries.* Annual review of energy and the environment, 1998. **23**(1): p. 253-286.
20. Tilley, E., *Compendium of sanitation systems and technologies*. 2008: Eawag.
21. Neville, R.C., *Solar energy collector orientation and tracking mode.* Solar energy, 1978. **20**(1): p. 7-11.
22. Castiglia-Feitosa R. and Wilkinson S., *Retrofitted Green Roofs and Walls and Improvements in Thermal Comfort*, Workshop of Off-grid Technology Systems, AIP Conf. Proc. 1856, 020006 (2017).
23. Morrissey, J., T. Moore, and R.E. Horne, *Affordable passive solar design in a temperate climate: An experiment in residential building orientation.* Renewable Energy, 2011. **36**(2): p. 568-577.
24. Shaviv, E., A. Yezioro, and I.G. Capeluto, *Thermal mass and night ventilation as passive cooling design strategy.* Renewable energy, 2001. **24**(3): p. 445-452.
25. Aksoy, U.T. and M. Inalli, *Impacts of some building passive design parameters on heating demand for a cold region.* Building and Environment, 2006. **41**(12): p. 1742-1754.
26. West, S. *Innovations from Scandinavia: Increasing the Potential for Reuse*. 2001. On-site.
27. Kol, H.Ş., *Thermal and dielectric properties of pine wood in the transverse direction.* BioResources, 2009. **4**(4): p. 1663-1669.
28. McLennan, J.F., *The philosophy of sustainable design: The future of architecture*. 2004: Ecotone publishing.
29. Australia, S., *Structural design actions Part 0: General Principles*, in *AS/NZS 1170.0:2002*. 2002: Australia/ New Zeland.
30. Australia, S., *Structural design actions Part 1: Permanent,imposed and other actions*, in *AS/NZS 1170.1:2002*. 2002: Australia/ New Zeland.
31. Australia, S., *Structural design actions Part 2: Wind Actions*, in *AS/NZS 1170.2:2011*. 2011: Australia/ New Zeland.
32. Australia, S., *Structural design actions Part 4: Earthquake actions in Australia*, in *AS/NZS 1170.4:2007*. 2007: Australia/ New Zeland.
33. Wood, J., P. Pockets, and B. Peck, *Mechanical properties of wood.* Aging, 1999. **4**: p. 41.
34. Institute of Australian Geographers, *Australian geographical studies*. 2004.

Polypyrrole Functionalized with Carbon Nanotubes as an Efficient and New Electrodes for Electrochemical Supercapacitors

Kakarla Raghava Reddy[1,2, a)] *and Fernando Alonso-Marroquin*[2)]

[1]*School of Chemical and Biomolecular Engineering, The University of Sydney, Sydney, NSW, Australia*
[2]*School of Civil Engineering, The University of Sydney, Sydney, NSW, Australia*

[a)] *Corresponding author: reddy.chem@gmail.com*

Abstract. This study evaluates the effectiveness of chemical functionalization of multiwalled carbon nanotubes (MWCNTs) with polypyrrole (PPy) via chemical oxidative polymerization on the electrical conductivity and electrochemical supercapacitive properties of the PPy-MWCNTs functional hybrids. They demonstrate good specific capacitance up to 268 F/g at a current density of 1 A/g and a good cycling stability, which is higher than that of pure PPy. These advanced electrodes can be used as high-performance electrochemical energy storage supercapacitors.

1. INTRODUCTION

Since discovered by Iijima in 1991, [1] carbon nanotubes (CNTs) have been the subject of many studies due to their unique thermal, catalytic, mechanical and electrical properties. They can be used for a wide range of application such electronic devices, solar cells, supercapacitors, transparent electrodes, chemical sensors, field emission displays, off grid technologies, high-surface-area electrodes and high-performance nanotube-reinforced composites [2-6]. Among them, electrochemical supercapacitors are charge storage devices that possess high density and longer cycle life than the normal batteries and conversional supercapacitors. The energy storage mechanism in supercapacitors is usually Faradic and electrical double-layer. Recent research efforts have been focused on improving the electrical and electrochemical properties of carbon nanotubes for the energy storage applications by developing novel electrode materials [7-9]. These energy storage devices are widely used in consumer electronics due to their higher specific energy and power density, and they have a potential power source for efficient offgrid systems and electronic vehicles in the future. However, pristine CNTs cannot meet the commercial requirements for these applications due to its poor dispersion in solvents and low electrochemical characteristics in the electrolytes.

Chemical modification of CNTs such as acid treatment, oxidation and plasma etching to produce functional groups, including carboxylic groups, ester, zwitterions, have been reported on the surface of CNTs to improve electrical properties [10, 11]. Oxidation can occur during CNTs purification with the reaction of strong acids. Existing of these functional groups on the CNTs surface could enhance interactions of nanotubes and charge-carrying capability [12]. The acid-treated CNTs conductivity can be enhanced, resulting in the addition of charge carriers either in the form of p-type and n-type doping. Acidic dopants convert the semiconducting nanotubes into conducting type through effective tuning of the nanotubes in Fermi level through either changing the conduction or valance bands with electron doping and hole doping. CNT Fermi levels were tuned by chemical treatment, thereby increasing the intrinsic conductivity of the CNTs while decreasing the inter-tube resistance through mitigation of Schottky barrier. Thus, acidic-doped nanotubes show relatively higher electrical conducting properties after being treated with strong acids such as HCl, HNO_3 and H_2SO_4. It is also showed that tangential mode of metallic CNTs in Raman Scattering measurements depended sensitively on the exposure to HNO_3 oxidation reaction [13]. It is due to charge transfer doping by acidic reaction. In device fabrication processes, doped CNTs have to go through metal deposition and encapsulation processes, etc. These processes may involve exposure to various solvents and open air,

Off-Grid Technology Workshop
AIP Conf. Proc. 1856, 020002-1–020002-4; doi: 10.1063/1.4985553
Published by AIP Publishing. 978-0-7354-1530-0/$30.00

as well as elevated temperature conditions. Furthermore, actual device operation may also need the doped CNTs to work in open air and elevated temperatures. Therefore, doping stability, lower cycle-life and not stable during the redox process are issues for acid-treated CNTs. Hence, it is necessary to protect CNTs with support layer in order to demonstrate an improved stability and electrical properties at open air and elevated temperatures.

Electrically conducting polymers (e.g., polyaniline, polypyrrole, polythiophene, polyanisidine, polytoluidine and their derivatives, co- and terpolymers) used as electrode materials for energy storage systems that have several advantages due to their fast charge-discharge characteristics, low cost, suitable morphology, and fast doping-dedoping process [14-16]. Among various conducting polymers, polypyrrole (PPy) is easy to synthesize, highly mobility of charge carriers in extended π-conjugated electronic systems, good conductivity in doped state, thermally stable and environmentally friendly. Therefore, it is important to develop electronically coupled polymers with nanotubes that allow fabrication of large scale in power or highly flexible form of storage devices with excellent specific capacitance and long cycle-life. The interaction of CNTs with conducting PPy can provide more electron migration pathway, reduce the resistance, and increase absorption characteristics due to their rough surface. However, to best of our knowledge, there are no studies that investigated chemically functionalized CNTs-PPy hybrids for the supercapacitors.

In this work, for the first time, we report for the functionalization of CNTs with polypyrrole through *in-situ* chemical oxidative polymerization in the presence of sulforhodamine B as dopant and self-organizing agent, and investigated their structural, morphological, electrical conducting and supercapacitive properties.

2. Experimental

Initially, multi-walled carbon nanotubes (MWCNTs) were prepared by CVD process, and purified them by treating them with 12M HNO_3, followed by washing with excess of deionized water. Purified product was dried under vacuum for 24 h. The synthesis of MWCNTs-functionalized PPy through in-situ chemical oxidative polymerization process is as follows. Certain amount of purified MWCNTs was placed into the deionized water that containing 0.27 mmol of sulforhodamine B and 4.47 mmol of pyrrole monomer, and stirred the solution for an hour. Then, 10 mL of $FeCl_3$ (1.668 gm) was added to above dispersion by drop-wise and stir for 12 hours. After completion of polymerization reaction, predicated product was washed for three times with deionized water and ethanol, and dried under vacuum at 40 °C for 12 hours. For comparison purpose, pure PPy polymer was synthesized under similar conditions without using MWCNTs.

2.1. Characterization methods

MWCNTs-functionalized PPy hybrids containing different Wt% of purified carbon nanotubes were analyzed for their structural, electrical conducting and electrochemical supercapacitive properties by using FE-SEM, FTIR, Four-probe meter, CV and EIS, respectively.

3. Results and Discussion

3.1. Formation of the MWCNTs-PPy Hybrids and its Structural Characterization

The size and morphological structures of purified MWCNTs and MWCNTs-functionalized PPy hybrids were characterized by using FE-SEM. Figure 1A shows that diameter of nanotubes is 10-15 nm with the length of few microns. After acidic treatment, MWCNTs are purified without having any impurities. The morphology of the nanotubes dramatically changed after the functionalization with PPy. The nanotubes are encapsulated in the polymer matrix that can be clearly seen in Figure 1B. Most of the long nanotubes are wrapped with the PPy due to strong interactions between the functional groups of CNTs and PPy.

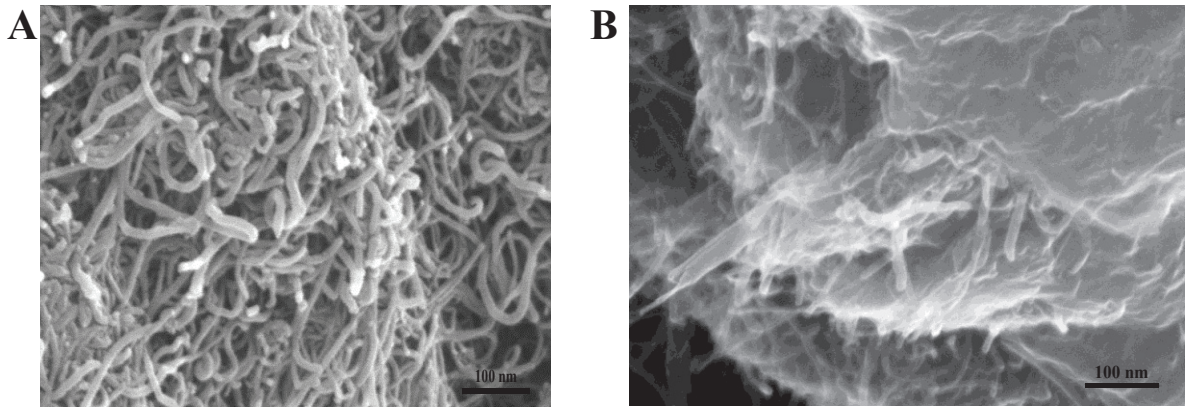

FIGURE 1. FE-SEM images of (A) purified MWCNTs, and (B) MWCNTs-functionalized PPy composites.

The mechanism for the formation of MWCNTs-PPy hybrids is as follows. Initially, purified MWCNTs that prepared by oxidation reaction with nitric acid, are dispersed in solution containing pyrrole monomer and sulforhodamine. During this process, nanotubes adsorb pyrrole molecules, and sulforhodamine present in the reaction system act as both organic dopant and self-organizing agent. They form complex with pyrrole through the interactions between $-SO_3H$ groups of sulforhodamine and amino groups of pyrrole, and that complex leads to formation of micelles in the system and increase the rate of the reaction. Since it simultaneously functions as an organic dopant, it increases the electrical conducting and electrochemical properties of MWCNTs-PPy hybrids. When iron chloride added by dropwise to the reaction, pyrrole molecules undergo polymerization reaction and grow on the surface of carbon nanotubes. As a result, the MWCNTs-PPy hybrids were formed through in-situ chemical oxidative polymerization process.

To confirm the successful polymerization of pyrrole monomer and presence of PPy in the composite hybrid, FTIR analysis of the pristine PPy and MWCNTs-PPy hybrids were performed. Pristine PPy (Figure 2a) showed major peaks at 1545, 1472, 1295, 1100, 1040 and 930 cm^{-1} which are attributed to pyrrole ring and conjugated C-N stretching, N-H deformation, out-of-plane vibrations of C-H and ring deformation. All these peaks of PPy are reflected in the composites (Figure 2b) with some shifts in wavelength. This indicates that pyrrole was polymerized by *in-situ* chemical oxidation process, and exists in the composites without damaging the backbone structure of polymer.

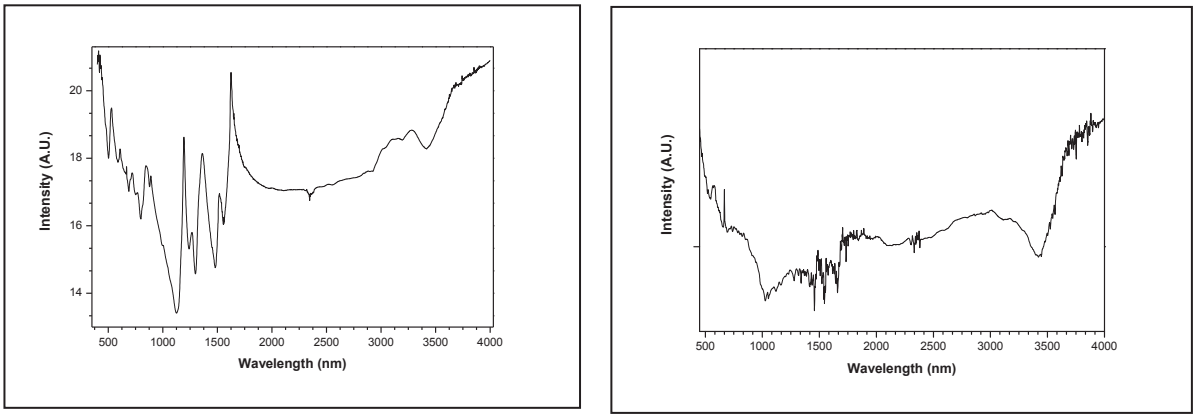

(a) (b)

FIGURE 2. FTIR spectra of (a) pristine PPy, and (b) MWCNTs-PPy composites.

We also used Raman study to determine electronic structure of the composites. We found that the intensity of G and D bands increased, and the ratio of the intensity of the D band to the intensity of the G band was smaller for the MWCNTs-PPy hybrids than pure carbon nanotubes. This is due to formation of polymer on carbon nanotubes

eliminates the defect sites of nanotubes. Moreover, the dispersion of nanotubes in the polymer matrix did not change the electronic energy states of the CNTs in the composites.

The influence of CNTs content (Wt%) on the electrical conducting and supercapacitive properties of the MWCNTs-PPy composites were investigated as shown in the Table 1. Pristine PPy shows the electrical conductivity of 0.83 S/cm. When PPy is combined with nanotubes, the electrical conductivity and supercapacitive properties of the composites were significantly increased with increasing the Wt% of CNTs. This is due to effective dispersion of nanotubes in the polymer matrix that favors the electronic transport, and change in the morphological structures as observed from SEM results. Higher capacitance for the composites is due to a synergistic effect between PPy and CNTs. CNTs present in the composites act as an efficient electrode material to increase the capacitance and promote the insertion of electrolyte ions in the composites for charge-discharge process, and PPy can promote the charge transportation. We found that specific capacitance values were not much enhanced beyond the 12 Wt.% of CNTs. Composite with 12 wt% of CNTs showed maximum capacitance of 268 F/g with 76% capacitance retention after 3000 cycles.

TABLE 1. The conductivity and specific capacitance of the MWCNTs-PPy hybrids.

PPy-MWCNTs Nanohybrids	Conductivity (S/cm)	Specific Capacitance (F/g)
Pristine PPy	0.83	116
PPy-MWCNTs-3	1.97	158
PPy-MWCNTs-8	4.22	234
PPy-MWCNTs-12	6.82	268

4. CONCLUSIONS

We have successfully synthesized MWCNTs-functionalized polypyrrole and investigated the influence of carbon nanotubes on the electrical conducting and the electrochemical capacitive behavior of the MWCNTs-PPy composites. It is found that composites have excellent conductivity and maximum capacitance of 268 F/g. Moreover, the device showed good cycle-stability. Such novel electrodes are promising candidates for high-performance energy storage applications.

REFERENCES

1. S. Iijima, Nature **354**, 56-58 (1991).
2. K. Aitola, S. Kari, J. Correa-Baena, A. Abate, Y. Tian, M. Grazel, A. Hagfeldt and G. Boschloo, Energy Environmental Sci. **9**, 461-466 (2016).
3. H. Yuan, Q. Jiao, S. Zhang, Y. Zhao, Q. Wu and H. Li, J. Power Sources, **325**, 417-426 (2016).
4. V. D. Dao, L. L. Larina, J. K. Lee, K. D. Jung, B. T. Huy and H. S. Choi, Carbon, **81**, 710-719 (2015).
5. M. Baghayeri, A. Amiri and S. Farhadi, Sensors and Actuators B: Chemical, **225**, 354-362 (2016).
6. A. Rabti, N. Raouafi, A. Merkoci, Carbon, **108**, 481-514 (2016).
7. M. Cakici, K. R. Reddy and F. Alonso-Marroquin, Chemical Eng. J. **309**, 151-158 (2017).
8. Z. Qiu, D. He, Y. Wang, X. Zhao, W. Zhao and H. Wu, RSC Adv. **7**, 7843-7856 (2017).
9. W. Liu, Y. Tang, Z. Sun, S. Gao, J. Ma and L. Liu, Carbon, **115**, 754-762 (2017).
10. A. Morelos-Gomez, I. Ito, T. Fukuyo, K. Fujisawa, T. Fujimori, K. Kaneko, T. Hayashi, M. Endo and M. S. Dresslhaus, J. Mater. Chem. A. **4**, 74-82 (2016).
11. D. Janas, S. K. Kreft and K. K. K. Koziol, Materials & Design, **116**, 16-20 (2017).
12. K. R. Reddy, B. C. Sin, K. S. Ryu, H. Chung and Y. Lee, Synthetic Metals, **159**, 595-603 (2009).
13. D. Zhang, J. Yang, M. Li and Y. Li, ACS Nano, **10**, 10789-10797 (2016).
14. T. Chen, Y. Huang, C. Li, C. Kung, R. Vittal and K. Ho, Nano Energy, **32**, 19-27 (2017).
15. R. R. Kakarla, K. Nakata, D. A. Tryk and A. Fujishima, J. Nanosci and Nanotech. **10**, 7951-7957 (2010)
16. K. R. Reddy, K. P. Lee, A. I. Gopalan and A. M. Showkat, Polymer Journal, **38**, 349-354 (2006).

Graphene oxide functionalized with silver nanoparticles as conducting electrodes for solar cells and electrochemical energy storage devices

Kakarla Raghava Reddy[1,2, a)] *and Fernando Alonso-Marroquin*[2)]

[1]*School of Chemical and Biomolecular Engineering, The University of Sydney, Sydney, NSW, Australia*
[2]*School of Civil Engineering, The University of Sydney, Sydney, NSW, Australia*

[a)] *Corresponding author: reddy.chem@gmail.com*

Abstract. We present the development of novel electrochemical supercapacitor and sensor based on silver (Ag) nanoparticles coated graphene oxide (GO). 10-20 nm diameter of Ag nanoparticles were well dispersed on the surface of graphene oxide through the chemical reduction method. Ag-coated GO nanohybrids were characterized by transmission electron microscopy (TEM), X-ray diffraction, Raman spectroscopy, electrical and an electrochemical analysis for the energy storage (supercapacitors), energy conversion (solar cells) and sensor applications. It is found that nanohybrid electrodes showed good specific capacitance and electrochemical sensing performance in comparison to pristine GO. The improvement in the electrochemical characteristics can be attributed to the sensitizing effect between Ag nanparticles and GO. These GO/Ag hybrid transparent conducting films also show low resistance and good transmittance, suggesting they are good electrodes for the opto-electronic devices (e.g. solar cells).

1. INTRODUCTION

Nano optoelectronics such as photodetectors, energy conversion, energy storage and sensor devices have evolved extremely for the past few years, in design, fabrication and function [1-2]. Some of the inorganic semiconductors that use for such applications are Si, Ge, CdS, MnS, CdSe, CdTe, ZnO, TiO_2 and nanocarbons-based functionalized heterostructured materials. Inorganic semiconductors are known with tunable physical, thermal and opto-electronic properties that provide the charge-carrier characteristics for the applications in solar energy harvesting, light-emitting diodes (LEDs), photocatalysis and other nano-electronics devices. In the heterostructured inorganic nanohybrids (e.g. Cu_2S/conducting polymer, TiO_2/nanocarbon) for use in solar cells, the presence of interface between two components plays a key role in exciton dynamics in which the wavefunction of the charge-carrier confinement varies abruptly. In addition to that, heterostructure of nanohybrid shows good quantum yield of photoluminescence, enhanced charge separation yield, high transparencies, and high excited-state lifetime with strong solar conversion efficiency compared with pure or individual inorganic nanoparticles. Such heterostructured nanohybrids are also used for the energy storage and sensor devices as demonstrated by several researchers [2, 3]. The chemical structures, size, morphologies, properties and device characteristics will vary depending on the type of inorganic nanoparticles, which have a dazzling future in the nano opto-electronic industry.

Electrochemical supercapacitor energy storage systems have potential applications in development of wide range of electrical devices such as memory backup devices, hybrid electric vehicles, digital and portable electronic devices which is due to their outstanding electrochemical performance such as high energy density, high power density, specific capacitance, fast charging-discharging mechanism as well as long cycle life with high durability [3-5]. However, the energy density of supercapacitor is low compared with rechargeable batteries. Hence, researchers are trying to improve their energy densities to reach those of batteries. Various physical and wet chemical methods used to prepare various carbon nanostructured materials such as carbon black, activated carbon, 3D graphene sheets, 1D carbon nanotubes, porous carbons, graphene quantum dots, nanodiamond, porous carbons, onions-shaped carbons, 2D carbons, etc [6-10]. Among them, graphene has outstanding thermal, mechanical and electrical properties due to

Off-Grid Technology Workshop
AIP Conf. Proc. 1856, 020003-1–020003-5; doi: 10.1063/1.4985555
Published by AIP Publishing. 978-0-7354-1530-0/$30.00

their high surface area and nanostructures [11-13]. They are low-cost, easy synthesis, production in large quantity, and excellent renewable carbons for energy storage and sensor applications [14, 15].

Different materials such as polyaniline, polypyrrole and polythiophene have been used for the electrochemical sensors and energy storage devices [16-18]. It's due to their good properties such as good stability under ambient conditions, good electrical conductivity, chemical and thermal stability which allows applying it as an electron relay. Composites were prepared based on polypyrrole and graphene oxide for the sensors [19]. GO coated with polyaniline has been used as binder-free electrodes for electrochemical supercapacitors [20]. They shows specific capacitance of 385 F/g at 0.5 A/g and 243 F/g at 1 A/g. 3D porous GO foam was prepared using nickel foam as the hard template, polyaniline arrays was coated on the surface of GO for supercapacitors that shows high specific capacitance of 790 F/g and volumetric capacitance of 205 F/cm^3 at 1 A/g [21]. However, this process tedious process such as using sacrificial template method that hinders the mass-production. Polythiophene/nano-carbon/Pt composite electrode showed volumetric capacitance of 10 F/cm^3 in liquid and solid electrolytes at a scan rate of 10 V/s [22]. Other metal and metal oxides such as $NiCo_2O_4$, $ZnCo_2O_4$, MnO_2, $CoFe_2O_4$, etc has been used to improve the electrochemical performance of the electrodes [23-26].

Silver nanoparticles have excellent optical and electrical properties and they used in many potential applications such as immobilized enzyme, cell separations, cytotoxicity, targeting therapy and energy storage devices [27, 28]. However, the reports on GO-Ag based hybrid for both electrochemical energy storage devices and sensors are rare. Novelty of this work is to use same electrode materials for both applications with enhanced electrochemical performance of GO-Ag hybrid. Ag NPs functionalized GO hybrid was prepared, and characterized by TEM, XRD, Raman spectra and an electrochemical behavior using cyclic voltammetry (CV), Electrochemical Impedance Spectroscopy (EIS). The as-synthesized GO-Ag hybrid electrodes exhibit good specific capacitance with electrochemical stability, as well as good electrochemical biosensing for glucose. We further investigated GO/Ag hybrid films for their optical, electrical conducting and band-gap properties for solar cells applications.

2. Experimental

Initially, GO was prepared from the graphite as per our previous work [8]. Then, GO was dispersed in 20 mL of DI water containing $AgNO_3$ ($2x10^{-4}$ M), and sodium citrate ($1.7x10^{-3}$ M) that act as stabilizing agent. 0.6 mL of pre-prepared ice cold sodium borohydride solution was added to above solution by drop-wise and stir the mixed solution. Finally, GO-Ag hybrid is washed with DI water and ethanol to remove the impurities, filtered using membrane filter and dried in vacuum oven at 50 °C.

2.1. Characterization methods

GO-Ag nanohybrids were analyzed for their structural, optical, electrical conducting and electrochemical properties by using TEM, XRD, XPS, Raman, CV and EIS, respectively.

3. Results and Discussion

3.1. Morphology and Structural Properties of GO-Ag Nanohybrids

The size and morphological structures of GO-Ag nanohybrids were directly analyzed by using TEM, as shown in Figure 1. It clearly reveals that 10-15 nm size of silver nanoparticles was well dispersed on GO surface. These Ag particles on GO surface are uniform size with individually distributed. Charges present on the GO surface form complex with negative charges of Ag ions in the aqueous solution. When the addition of $NaBH_4$ as the reducing agent to aqueous solution, Ag ions are reduced to Ag particles on GO surface, resulting in the formation of GO-Ag nanohybrid. Since Ag particles are excellent electrical conductors, they improve the electrochemical characteristics of GO-Ag nanohybrid.

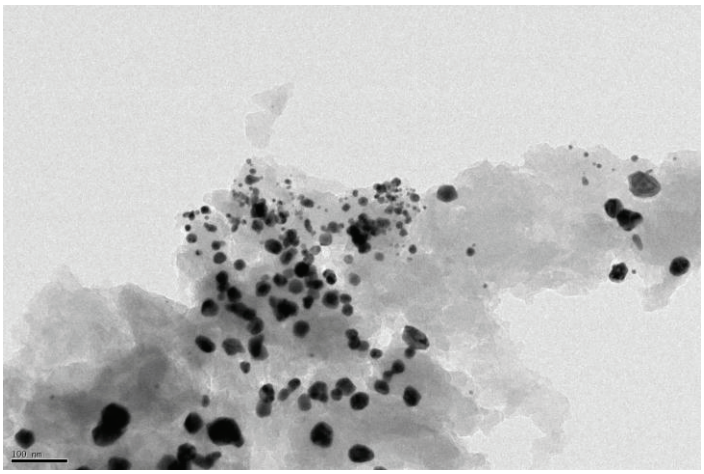

FIGURE 1. TEM image of Ag nanoparticles-functionalized GO hybrid. Scale bar is 100 nm.

To confirm the electronic structure of Ag nanoparticles coated-GO hybrid, Raman spectroscopy was performed and the data was presented in Figure 2. GO-Ag hybrid showed two strong peaks at 1350 and 1600 Cm^{-1} which are called as D and G bands. D band originates from the level of disordered carbons and G band originates from the Raman vibrational modes of graphite. It confirm from Raman results that the electronic structure of GO did not change upon coating with silver nanoparticles.

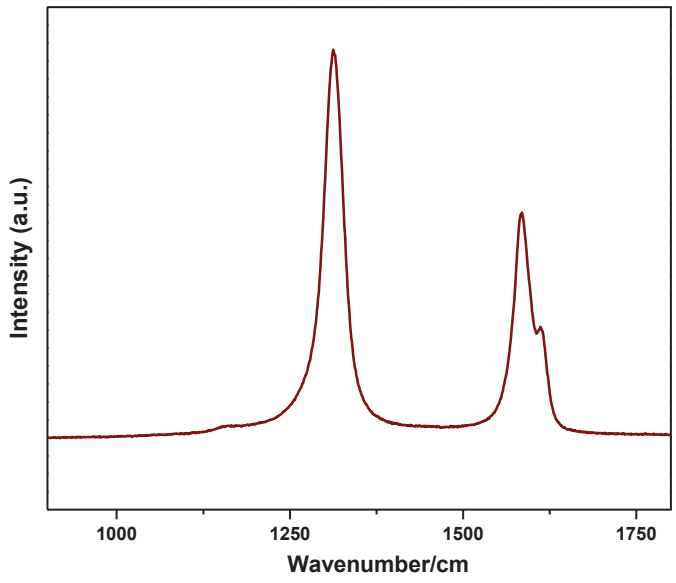

FIGURE 2. Raman spectra of GO-Ag nanohybrid.

3.2. Supercapacitor and Sensor Performance of GO-Ag Nanohybrids

The GO-Ag hybrids were tested for their use as electrodes for electrochemical supercapacitors and sensors. The cyclic voltammetry results of hybrid electrode showed that the curves with more quasi-rectangular behavior than that of pure GO. This indicates that better electrochemical performance for GO-Ag nanohybrid than that of pure GO. This is due to better electron transportation and enhanced electrical characteristics of GO after coating with Ag particles on their surface. The specific capacitance of GO-Ag hybrid electrode was 228 F/g at a current density of 0.5 A/g. After 2000 cycles, they exhibited the capacity retention of 74%. The good electrochemical capacitive performance of hybrid is due to i) change in the morphological heterostructure, ii) Ag particles can improve electrolyte osmosis and reduce the ionic diffusion parthway, iii) Ag particles in the composite favor the pathway for rapid charge storage and transfer.

Since Ag has excellent sensing ability, we also tested its electrochemical sensing performance for the detection of glucose. The composite solution was dispersed on the surface of an ITO electrode. 25 ul of GO_x was immobilized onto surface of GO-Ag hybrid. Pure GO/GO_x sensor device was also similarly tested for comparison. The CV results reveal that GO-Ag hybrid in the absence of glucose shows a pair of redox peaks that indicates that good electron transfer occur between the redox center of GO_x and the electrode surface. The hydrogen peroxide reduction current of hybrid electrode is higher than of pure Go electrode. The higher peak current for glucose for hybrid electrode is due to the difference between the isoelectric points of silver particles and GO_x. Therefore, this novel material can provide good enzyme adsorption through direct electron transfer between the redox sites of enzyme and the surface of electrode. The reason for this is Ag particles on GO surface can greatly enhance the effective reactive area of electrode and Ag particles promote the electron transfer. Hence, this material can be potential biosensor with good stability.

3.3. Band-gap and opto-electronic properties of GO/Ag hybrid films

Since carbon nanostructured materials are transparent conducting electrodes, they play key role in the large scale opto-electronic devices such as photovoltaic devices, light-emitting diodes LED), solar cells, photoanodes for hydrogen generation, etc. Current LED electrodes are developed by using indium tin oxide (ITO) as it has excellent electrical conducting, photoelectrochemical properties and remarkable optical transmittance. However, they have limitations that restrict for practical industrial applications due to high cost, less durability, and diffusion of In element into the light-emitting layer. We have used efficient functionalization method to uniformly coat silver nanoparticles on the surface of graphene oxide. The monodispersed noble metal particles present on graphene oxide further significantly enhances the photo-electrochemical properties of GO/Ag hybrid electrodes due to unique properties of silver nanoparticles with an excellent electrical conductivity (6.3×10^7 S/m), thermal stability and optical characteristics as well as their potential use in a wide range of applications in the nano-electronic devices. Another promising candidate material is graphene to replace ITO transparent electrodes due to large surface area and electrical properties. Combining graphene oxide with silver particles, GO/Ag hybrid can provide both outstanding optical and electrical properties. We except that these opto-electrical characteristics are useful to fabricate quality transparent electrode devices with excellent luminous efficiency. Therefore, we attempted to investigate graphene-Ag based composites as an alternative transparent conducting electrode for photoelectrochemical applications. Our GO/Ag hybrid transparent conducting films show low resistance of 42 Ohms/sq and good optical transmittance in the visible region. These preliminary results reveal that GO/Ag composite transparent conducting films can be used as an alternative promising candidate to replace conventional ITO in opto-electronic devices such as solar cells, photovoltaic devices and photoanodes for water splitting to generate hydrogen. Optical transparency behavior in the nanohybrid is an important benefit of solar cells for wide range of practical applications such as windows, roof panels or various decorative large installations. We also used XPS to determine the electronic properties of GO/Ag hybrid. GO/Ag hybrid shows the Ag $3d_{5/2}$ and Ag $3d_{3/2}$ bands at 367.2 and 373.5 eV that are attributed to binding energies of Ag element. The difference between two bands is 6.3 eV. This is caused by the electron transfer from Ag to GO. Since the work function of Ag (4.2 eV) is smaller than that of graphene (4.8 eV), the electron transfer from Ag nanoparticles to GO automatically take place in the GO/Ag hybrid film. This would lead to effective doping GO with Ag through more electrons and improve its Fermi level above the conical point, and changes band-gap engineering behavior.

4. CONCLUSIONS

Ag nanoparticles functionalized GO was successfully synthesized through the sodium citrate chemical reduction method. They synthesized GO-Ag nanohybrids showed good electrochemical properties such as good specific capacitance and good cycling stability. Moreover, hybrid electrodes showed good performance as biosensor for the detection of glucose. The excellent electrochemical characteristics indicate that novel GO-Ag hybrids are promising electrode materials for the electrochemical energy storage and biosensors. These transparent GO/Ag films also show good photo-electrochemical properties, suggesting that these films are promising candidates as the transparent conductive electrodes in devices such as solar cells.

REFERENCES

1. L. Cui, J. Gao, T. Xu, Y. Zhao and L. Qu, Chemistry an Asian Journal **11**, 1151-1168 (2016)
2. W. Zhang, S. Yang, J. Li, W. Gao, Y. Deng and W. Dong, Appl. Catalysis B. Environmental **206**, 89-103 (2017).
3. M. Sevilla and A. B. Fuertes, ChemSusChem **9**, 1880-1888 (2016).
4. C. Hu, E. Zhao, N. Nitta, A. Magasinski and G. Yushin, J. Power Sources **326**, 569-574 (2016).
5. W. Li, S. Wang, L. Xin, M. Wu, X. Lou, J. Mater. Chem. A. **4**, 7700-7709 (2016).
6. D. R. Son, A. V. Raghu, R. R. Kakarla and H. M. Jeong, J. Macromol. Sci. Part B: Physics, **55**, 1099-1110 (2016).
7. K. R. Reddy, V. G. Gomes and M. Hassan, Materials Research Express, **1**, 015012 (2014).
8. S. H. Choi, D. H. Kim, A. V. Raghu, H. I. Lee, K. S. Yoon, H. M. Jeong, and B. K. Kim, J. Macromol. Sci. Part B: Physics, **51**, 197-207 (2012).
9. K. R. Reddy, B. C. Sin, K. S. Ryu, J. Noh, Y. Lee, Synthetic Metals, **159**, 1934-1939 (2009).
10. J. Patino, N. L. Salas, M. C. Gutierrez, D. Carriazo and F. Monte, J. Mater. Chem. A. **4**, 1251-1263 (2016).
11. Y. R. Lee, S. C. Kim, H. I. Lee, A. V. Raghu and H. M. Jeong, Macromol. Res. 19, 66-71 (2011).
12. X. Cui, P. Ren, D. Deng, J. Deng, X. Bao, Energy Environ. Sci. **9**, 123-129 (2016).
13. P. Ruffieux, S. Wang, B. Yang, J. Liu, T. Dumslaff and K. Mullen, Nature **531**, 489-492 (2016).
14. J. Yun, Y. Lim, G. N. Jang, D. Kim, S. Lee and J. S. Ha, Nano Energy 19, 401-414 (2016).
15. M. Hirtz, A. Oikonomou, N. Clark, H. Fuchs, and A. Vijayaraghavan, Nanoscale, 8, 15147-15151 (2016).
16. M. C. Tu, H. K. Svm, A. Thilini, A. Palaniappan and B. Liedberg, Sensors and Actuators B: Chemical, **247**, 916-922 (2016).
17. Y. Zhang, B. R. Bunes, C. Wang, N. Wu and L. Zang, Sensors and Actuators B: Chemical **247**, 713-717 (2017).
18. K. R. Reddy, K. P. Lee, A. I. Gopalan and A. M. Showkat, Polymer Journal, **38**, 349-354 (2006).
19. K. Koirala, F. B. Sevila and J. H. Santos, Sensors and Actuators B: Chemical **222**, 391-396 (2016).
20. Y. Meng, K. Wang, Y. Zhang and Z. Wei, Adv. Mater. **25**, 6985-6990 (2013).
21. P. Yu, X. Zhao, Z. Huang, Y. Li, Q. Zhang, J. Mater. Chem. A. **2**, 14413-14420 (2014).
22. J. A. Lee, M. K. Shin, S. H. Kim, H. U. Cho, G. M. Spinks, R. H. Baughman and S. J. Kim, Nat. Commun. **4**, 1970 (2013).
23. M. Cakici, K. R. Reddy and F. Alonso-Marroquin, Chemical Eng. J. **309**, 151-158 (2017).
24. Q. Wang, X. Wang, J. Xu, and D. Hou, Nano Energy **8**, 4451 (2014).
25. L. Lv. Q. Xu, R. Ding, L. Qi and H. Wang, Mater. Lett. **111**, 35-38 (2013).
26. Z. Wu, Y. Zhu, and X. Ji, J. Mater. Chem. A. **2**, 14759 (2014).
27. J. Huang, Z. Xie, Z. Xie, S. Luo, L. Xie, and T. Zeng, Analytica Chimica Acta **913**, 121-127 (2016).
28. D. R. Raj, S. Prasanth, T. V. Vineeshkumar and C. Sudarsanakumar, Sensors and Actuators B: Chemical **224**, 600-606 (2016).

Efficiency of the DOMUS 750 Vertical-Axis Wind Turbine

Kyle Hallock[1,2], Tyler Rasch[1,2], Guoqiang Ju[1], and Fernando Alonso-Marroquin,[1,a]

[1)] School of Civil Engineering, The University of Sydney, Sydney NSW 2006
[2)] College of Engineering, Boston University, Boston, MA 02215

[a)] Corresponding author: fernando@sydney.edu.au

Abstract. The aim of this paper is to present some preliminary results on the efficiency of a wind turbine for an off-grid housing unit. To generate power, the unit uses a photovoltaic solar array and a vertical-axis wind turbine (VAWT). The existing VAWT was analysed to improve efficiency and increase power generation. There were found to be two main sources of inefficiency: 1. the 750W DC epicyclic generator performed poorly in low winds, and 2. the turbine blades wobbled, allowing for energy loss due to off-axis rotation. A 12V DC permanent magnet alternator was chosen that met the power requirements of the housing unit and would generate power at lower wind speeds. A support bracket was designed to prevent the turbine blades from wobbling.

INTRODUCTION

A vertical-axis wind turbine is a device that generates power by converting kinetic energy from wind into electricity. What distinguishes a vertical-axis turbine from the more common horizontal variety is that the axis of rotation of a VAWT is perpendicular, rather than parallel, to the wind flow. VAWT systems are generally to be installed in small spaces, making them ideal for rooftop applications. Also, VAWT systems capture wind from all directions, so they are well-suited to work in variable conditions (Bellarmine and Urquhart, 1996).

The housing unit being built in the Off-Grid Technology Lab is designed to function as a habitable dwelling independent of power, water, and waste infrastructure. Preliminary testing has been done on the existing power systems – the solar array and VAWT – to determine how much power can be expected to be generated by both systems. The total energy required per day was estimated to be 0.69 kWh, and the existing solar power system generated 0.641 kWh per day. This results in an energy demand that exceeds 0.049kWh per day generated by the wind turbine.

EXISTING DESIGN

The design of the DOMUS 750 wind turbine features a Darrieus design, which arranges the aerofoils so that they are set relative to the structure on which they are mounted, see Figure 1. This blade design is effective regardless of the wind direction and increases low-wind performance while maintaining efficiency in high winds. This design also allows for the rotor to spin many times faster than the wind speed, increasing energy production. The generator that comes with the DOMUS 750 is a 36V DC permanent magnet brushed motor, which is only 69x60mm in size. The compact design works well in the apparatus, but constrains the effectiveness of the wind turbine as a whole.

Off-Grid Technology Workshop
AIP Conf. Proc. 1856, 020004-1–020004-5; doi: 10.1063/1.4985556
Published by AIP Publishing. 978-0-7354-1530-0/$30.00

Currently the wind turbine is mounted to a steel base, but with the proper hardware the turbine can be mounted anywhere on the roof of the off-grid housing unit. Keeping the turbine on the base at ground level has helped with testing and adding small changes to the design. To implement the turbine into the power generation system in the house, the generator will need to be connected to a charge controller that will be able to harness useful energy from the turbine when the solar panels do not supply enough power while also being able to dump the excess power developed by the turbine when there is ample wind and sunlight.

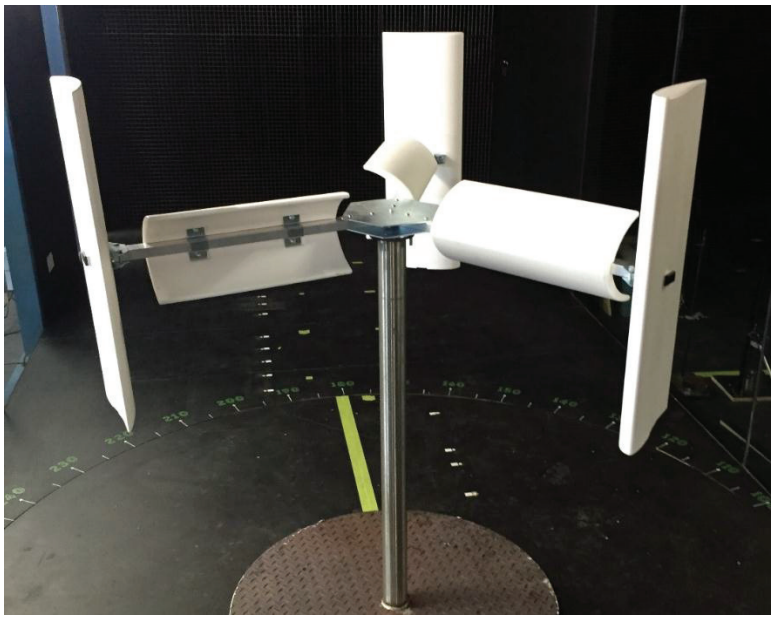

Figure 1. DOMUS 750 vertical axis wind turbine

TEST RESULTS

Here we summarize the main results obtained during the testing of the wind turbine. The wind velocity was increased from 0 to 19 m/s and then was decreased until zero. Figure 2 shows the rotational frequency versus wind speed. The start-up wind speed was 4 m/s. Above this speed the rotation frequency increases 7.2 RMP/(m/s). The noise produced by the turbine was moderated, with a range of 55 and 75 Decibels at one meter of the turbine. Figure 3 shows the the wind velocity vs power. it is shown that a linear increase in wind speed generates an exponential increase in power generation. In heavy winds the power generated is substantially more than in light winds. It is also important to note that because of the vertical axis, wind speed is much more important than wind direction.

Although it is not plotted on the above graph, the efficiency of the generator can be calculated for wind at 5m/s. Since the power generated is 0.003W, the calculated efficiency is only 6%. This must be greatly improved, since the current design only generates 0.000072kWh per day of the necessary 0.049kWh per day.

The turbine's efficiency comes predominantly from the generator that is currently being used. The generator has very poor low-wind performance, as it is designed for steady high wind applications. The generator has a large amount of resistance to motion, so it is hard to get the turbine spinning initially. While the generator has applications in other regions, Sydney has average wind speeds ranging from 2.3 to 3.9m/s, making the design ineffective for producing power (Bureau of Meteorology, 2017).

The other issue with the generator is the amount of play in the generator shaft. Because of the limited size, the generator shaft has enough deflection to cause an off-axis tilt of 4cm measured from the tip of the turbine blades.

This stem is not sturdy enough, and the energy lost due to the off-axis movement is substantial enough to reduce the system's rotational energy, leading to a large decrease in low-wind performance and efficiency.

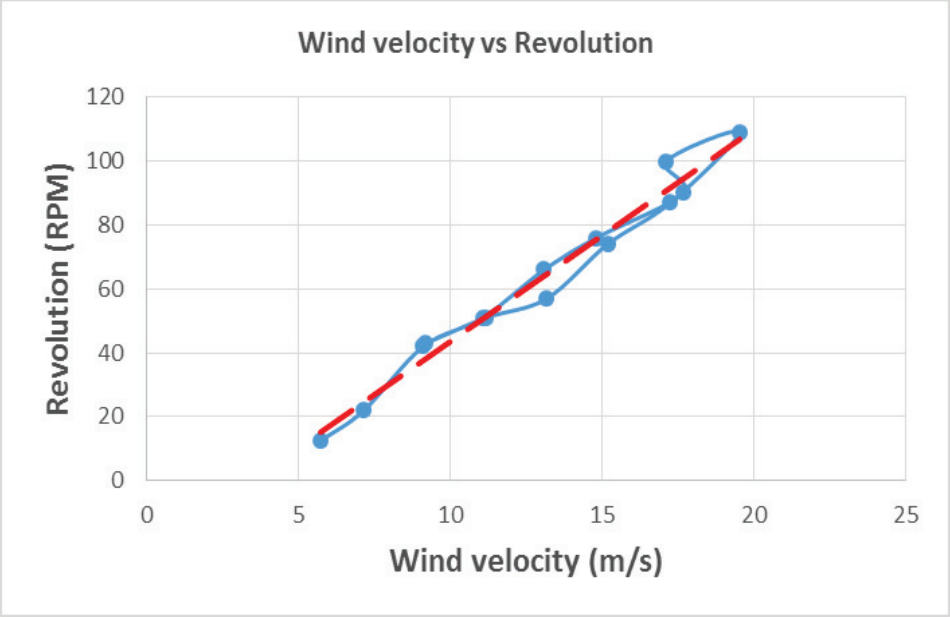

Figure 2. Angular frequency of the turbine versus wind speed.

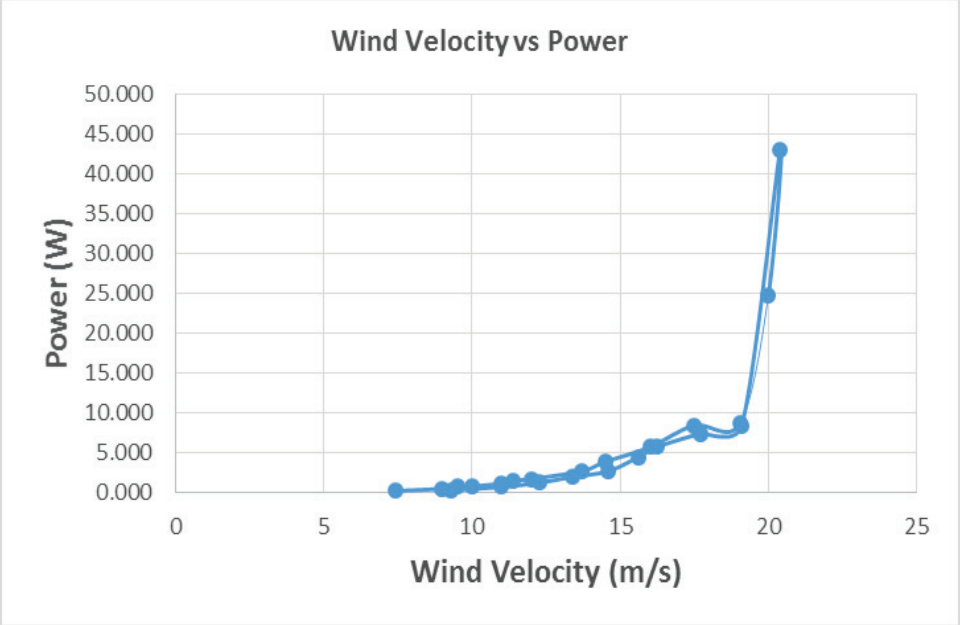

Figure 3. Power generated by the turbine versus wind speed.

DESIGN IMPROVEMENTS

The best option for fixing the efficiency issues of the turbine is to replace the generator with another popular option for VAWTs. By replacing the generator with one that requires less torque and has a smaller gear ratio would improve the low-wind performance of the turbine without hurting the performance in high wind scenarios. Below is a decision matrix of generator options, see Table 1. Each one of these alternative generators is a modified DELCO model generator, so each one is similar in size.

Table 1: Decision matrix of generator options

MODEL	Avg. Power Generation Capability	Start-up Wind Speed	Cost	Size	Peak Power Output at 1000 RPM
Wind Blue Power PMA DC-540	14V, 2A (28W) @ 150 RPM	~2.5 m/s	$285	16cm x 16cm Cylinder	1,170W
Missouri Wind and Solar 12V DC PMA	12V, 1.5A (18W) @ 150 RPM	"Very low"	$155	16cm x 16cm Cylinder	770W
Hurricane Wind Cat 4 Neo Core PMA	28V, 2.2A (61.6W) @ 200 RPM	~2.7 m/s	$320	16cm x 16cm Cylinder	1,691W
Current Generator: DOMUS 750	8.4W @ 100 RPM	~5 m/s	$0	Smaller than options listed above	N/A

The wobble issue will likely be remedied by replacing the generator with a more robust unit, but to make certain that the design will work shaft supports will be added to the turbine. A bracket will be attached to the connection between the blades and the generator shaft. The bracket will feature three L-shaped arms (Figure 4) that make contact with the turbine's vertical axis shaft via rollers (Figure 5). These rollers will have some friction reducing their effectiveness, but it will be much less energy loss when compared to the current wobble.

Figure 4. Bracket with L-shaped arms

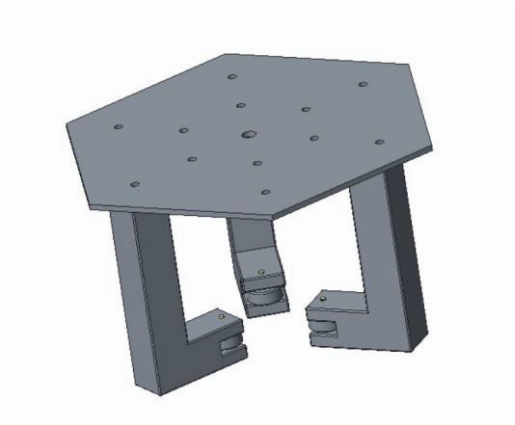

Figure 5. Turbine bracket attached to turbine

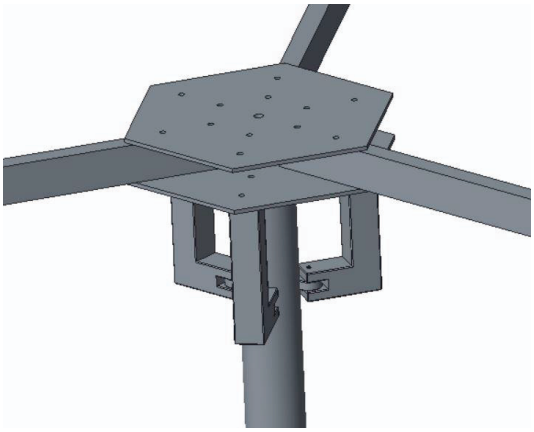

CONCLUSIONS

Based on the decision matrix for the new generator options, the option that most suits the needs of the project is the Missouri Wind and Solar Permanent Magnet Alternator (PMA). The 12V DC output can be easily added to the existing power storage system from the solar panel system. The generator also has been specifically designed for low wind startup, and is specifically designed for wind turbine usage. Given a higher budget, the Hurricane Wind Cat 4 Neo Core PMA is also a good choice, but the added benefit is not as substantial for its price point.

Replacing the generator with one of these options has issues, however. The DOMUS 750 generator which is currently being used is a much smaller size than the DELCO style generators which have been proposed. These much larger generators will likely require more parts to be machined in order to be mounted to the existing turbine framework. While this is a complicated addition to the project, other generators that are similar in size to the existing DOMUS 750 are exceedingly rare.

The stabilizing bracket and arms will be machined at the University of Sydney Civil Engineering workshop. The parts will be made from aluminium so that they retain their rigidity without being too heavy. This design might need to be changed if a larger generator is used in the turbine, as space near the generator shaft will be much tighter than at present.

ACKNOWLEDGMENTS

The experiments reported in this paper were performed in The Boundary Layer Wind Tunnel of the School of Civil Engineering of The University of Sydney.

REFERENCES

1. Australian Government Bureau of Meteorology. “Sydney (Observatory Hill).” *Monthly Climate Statistics.* Web. 18 May 2017.
2. G. T. Bellarmine, and J. Urquhart. "Wind energy for the 1990s and beyond." *Energy Conversion and Management* 37.12 (1996): 1741-752. *Elsevier*. Web. 2 Mar. 2017.
3. G. H. Herbert, S. Iniyan, E. Sreevalsan and S. Rajapandian. *A review of wind energy technologies*. Renewable and sustainable energy Reviews, 11(6), 1117-1145 (2007)

Vertical Garden for Treating Greywater

Arthur Phaoenchoke McDonald[1)], Alejandro Montoya[2)], and Fernando Alonso-Marroquin[1), a]

[1]*School of Civil Engineering, The University of Sydney, Australia.*
[2]*School of Chemical Engineering, The University of Sydney, Australia*

[a)]Corresponding author: fernando@sydney.edu.au

Abstract. Recent increasing concerns over the effects of climate change has prompted much debate into the issue of long term sustainability. An investigation was conducted into the feasibility of an off-grid housing unit, particularly in an Australian context. A pilot scale 3m ×2m off-grid housing unit was constructed. Forecasts for water requirements as well as an investigation into rainwater harvesting and greywater recycling was conducted. A multi-container plant and sand biological filter was constructed and filtration abilities investigated. The system met NSW government water reuse standards in terms of suspended solids and pH, achieving total suspended solid removal efficiency of up to 99%.

INTRODUCTION

With an increasing global water scarcity, the need for innovative and efficient technologies for water conservation is becoming increasingly essential. This research attempted to contribute to this effort by providing an investigation of rainwater harvesting and greywater recycling, in the specific context of an off-grid housing unit in Australia. Extensive literature review was conducted on rainwater harvesting to identify appropriate technologies and approaches to rainwater harvesting. Australia has one of the highest per capita domestic water consumption rates, currently at 223 liters per day (l/p/d) (Abs.gov.au, 2010). These figures are extremely high when compared to the average household water consumption rates of a similarly developed country, 124 (l/p/d) in the Netherlands (VEWIN, 2006). However, as water will be a particularly limited resource in off-grid housing project, minimum water requirements should also be examined. These estimates are presented in Table 1. As a result, this study used a reasonable water demand of 130 l/p/d for water balance calculations.

Table 1. Minimum Water Requirement Estimates (litres/person/day)

Drinking	Food Preparation	Sanitation	Bathing	Estimated Total	Study Author
Na	Na	Na	Na	20	(WHO/UNICEF, 2000)
5	10	20	15	50	(Gleick, 1996)
7.5	2	90.5		100	(Howard & Bartram, 2003)

Furthermore, conclusions can be made that an optimized rainwater harvesting system should consist of a smooth galvanized steel roof (Lee, et al., 2012) (Mendez, et al., 2011), first flush diverter discarding 2-5mm of first runoff (Kus, et al., 2010), virgin resin storage tank (Novak, et al., 2014), calming inlet and leaf shedding rain head. Combining average rainfall data and rainwater harvesting components, a spreadsheet was produced to forecast water balance. From the spreadsheet, it is evident that a large proportion of water consumption must be recycled to sustain the off-grid house. Thus, the need to combine greywater recycling with the rainwater harvesting system is imperative. Literature review was then also conducted on water recycling efficiencies of constructed wetlands, porous sand filters

Off-Grid Technology Workshop
AIP Conf. Proc. 1856, 020005-1–020005-10; doi: 10.1063/1.4985557
Published by AIP Publishing. 978-0-7354-1530-0/$30.00

and membrane filters. However, constructed wetlands and porous sand filtration appears most attractive, due to low energy demands. Furthermore, experimental designs of a pilot scale vertical forest (Constructed wetlands) and porous sand filter were compiled. In reality these experiments will require months to mature to its treatment potential. However, these experiments will help identify the most suitable solution for greywater treatment in an off-grid house in Sydney, Australia.

EXPERIMENT

Along with a pilot scale off-grid housing unit, a small-scale greywater recycling unit was constructed. This section portrays the processes and rationale taken to produce the pilot filtration system. A main motivation behind the project was to produce the system using very accessible materials and methods, whilst being fully self-sustainable within the off-grid housing unit. And so, most of the materials were sourced from readily available stores located in the inner Sydney region.

Materials and Setup

The design chosen was a hybrid between several systems available in the literature. The system draws on a constructed wetland by including aquatic plants, multi-layered porous sand filters as well as an activated carbon component. Four containers were connected in series; one being placed on top of the other. The greywater was drained from each box through a hole at the bottom of the container. To stop greywater exiting the system by flowing along the bottom of each container; a short hose was installed with silicon sealant to direct the effluent downwards. Fine plastic mesh was used to cover the hose's inlet to stop the possibility of gravel entering the hose. A diagram of the system is presented in Figure 1. The influent was retained in the plant container for different periods of time before being discharged into the lower containers. eventually flowing into the effluent container.

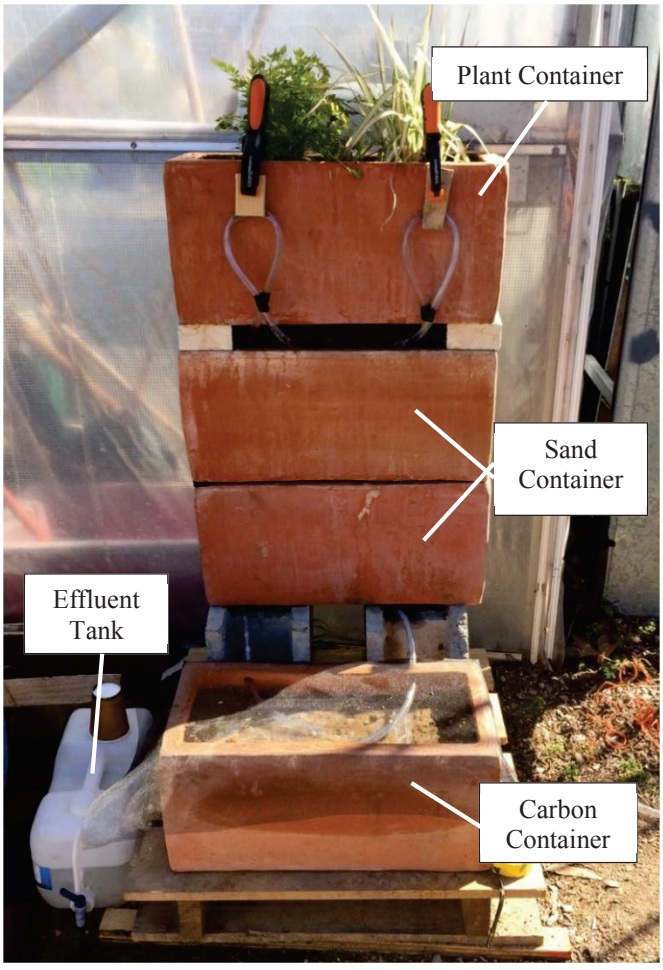

Figure 1 Experiment setup consisting on a vertical flow wet land, two sand containers, and a container with carbon activated material.

Influent Greywater

A synthetic greywater solution was used in place of household greywater for the influent. The synthetic greywater contains a mixture of water that has passed through a compost bin, lettuce vegetables, fungi and grease. A photo of the synthetic water is presented in Figure 2. Characteristics of the synthetic solution compared against typical grey water are presented Table1. As shown in Figure 2, the synthetic liquid presents indicators that are very similar to real greywater. However, other characteristics such as biological indicators were not conducted. Further research could be taken to conduct the experiment with various influent concentrations, especially at higher concentrations to provide greater insight into worst case scenarios.

Table 1. Influent Water Characteristics

Indicator	Synthetic Influent	Greywater	
TSS (mg/l)	42-60	25–183	(Li, et al., 2009)
TDS (mg/l)	184-229	137-1260	(Nghiem, et al., 2006)
EC (µs/cm)	355-461	401–495	(Masi, et al., 2010)
pH	6.41-6.93	6.3–8.1	(Li, et al., 2009)

Figure 2 Synthetic greywater mixture consisting of dirk, decay vegetables, and grease

Plant Box

The containers used in the experiment were 54cm × 27cm × 27cm terracotta pots. Terracotta was used as the porous clay allows air and moisture to penetrate through the sides. This natural aeration and the thick clay walls that stop rapid temperature changes, provide better conditions for biological filtration (University of Nebraska–Lincoln, 2008). Two types of aquatic plants were chosen for the experiment; Phalaris Arundinacea and Oenathe Sarmentosa (Water Parsley). These aquatic plants are cheap and easily accessible in local market. Two different types of plants were chosen to compare the growth responses to the greywater. If successful, the water parsley could also provide a food sources for the off-grid housing unit. The aquatic plants were placed in the container, as well as submerged in the synthetic greywater solution. This was done one month before conducting the experiments to help ensure sufficient time for roots to grow into the soil matrix. This was done as constructed wetlands typically require a few months for vegetation and biofilm establishment (Kaseva, 2004). In order to maintain a level of water within the plant's container at all times, the container's discharge tube was extended to ¾ height of the container, then returned to the sand container below. This was done to give some control over hydraulic retention times whilst maintaining sufficient water to sustain the aquatic plants. Gravel was placed to the bottom of each container to ensure adequate drainage

Three additional containers with porous media was used in the experiment. The same terracotta pot for the plants were used. Two of the pots contained washed sand while the remaining one contained sand and 2 kg of activated carbon. The activated carbon used was Aqua One® PremiumCarb, a phosphate free, aquarium grade activated carbon material. Being activated, the carbon contains a large amount of pores which significantly increase the surface area of the carbon, allowing better water purification. Similar to the plants, the two sand containers were submerged in the synthetic greywater solution for a period of 3 weeks. This was done to encourage the growth of the biofilm layer, known as the Schmutzdecke. The Schmutzdecke is known to develop after 14 days of loading (Campos, et al., 2002). In the same way as the plant containers, tubes were installed at the container's bottom to fully direct effluent discharge downwards. To ensure adequate drainage, 6mm gravel and 12-20mm pebbles were placed in sequence at the container's base, this is presented in Figure 3 and Figure 4.

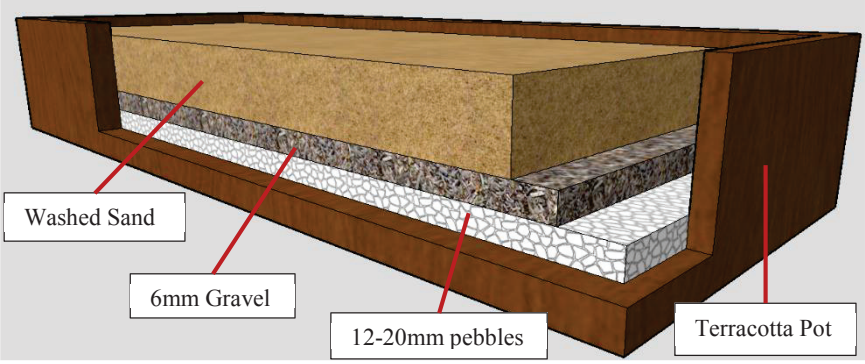

Figure 3 Sand Container Diagram

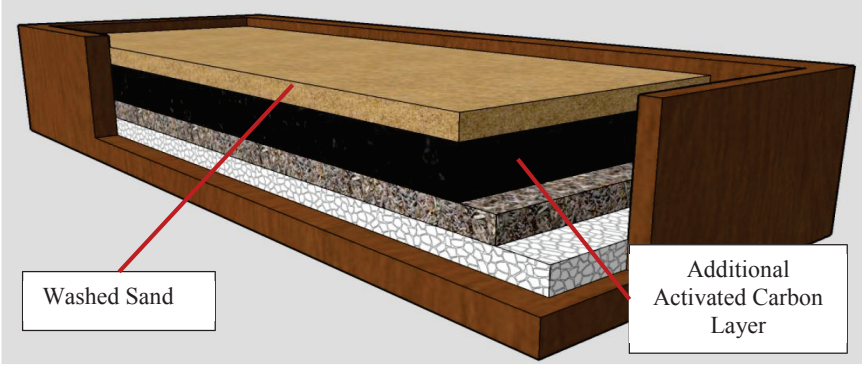

Figure 4 Activated Carbon Container Diagram

TESTS AND RESULTS

Retention times in the plant container was varied to investigate the effects of retention on water quality. Retention times used were 10 hours and 20 hours while an experiment with no retention was also conducted as a control. Measured water characteristics were pH, total dissolved solids (TDS), total suspended solids (TSS) and electrical conductivity (EC). After running each experiment, the effluent was collected in clear plastic bottles, and at the same time a sample of the synthetic effluent was also taken and stored in a plastic bottle. Values for TDS and EC were measured with a hand held instrument, "Excelvan® TDS & Conductivity meter". The instrument has an accuracy of ± 2% with a built-in temperature compensator. pH levels were measured with an Oakton® pH/CON 510 Benchtop Meter. The instrument has an accuracy of ±0.01pH.

Measurements for total suspended solids were also conducted by passing the effluent and influent through grade 2 filter paper. The weight of the filter paper was weighed prior to filtration. 100ml of the liquid sample was then

filtered through the paper with the aid of a vacuum chamber. The filtered paper was then dried at 101°C for 48 hours and then reweighed.

The amount of total suspended solids was then calculated using the equation below:

$$Total\ Suspended\ Solids\ (\frac{mg}{l}) = \frac{Weight\ after\ drying\ (mg) - Weight\ Initial\ (mg)}{liquid\ volumn\ (l)}$$

A visual presentation of the influent compared to the effluent is presented in Figure 5. The sample in the beaker labelled "In 3" being the influent of the 20-hr retention test, while the samples labelled 0, 10, 20 corresponds to the effluent's respected retention time. An image of the first sand container showing bio-layer growth is presented in Figure 6.

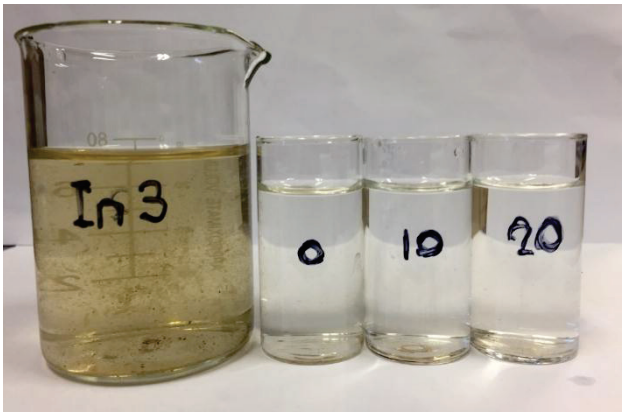

Figure 5 Influent and Effluent Samples

Figure 6 Bio-Layer Growth in Sand Container

Results from the experiment are summarized in Table 2. Greywater recycling requirements set by the NSW government as well as indicators for collected spring water from the Blue Mountains and rainwater are also included in Table 2. High exposure greywater reuse include uses for high levels of human contact, residential recirculation, agricultural irrigation for unprocessed foods and irrigation with unrestricted access (NSW Government, 2008).

Table 2 Summary of Experimental Results

Test	TSS (mg/l)	TDS (mg/l)	EC (µs/cm)	pH
Effluent (No Retention)	10.3 ±0.175	346 ±2%	693 ±2%	8.10 ±0.01
Effluent (10-Hr Retention)	1.70 ±0.142	444 ±2%	777 ±2%	7.45 ±0.01
Effluent (20-Hr Retention)	0.30 ±0.143	484 ±2%	965 ±2%	6.80 ±0.01
Spring Water	-	19 ±2%	38 ±2%	6.70 ±0.01
Rainwater	-	1 ±2%	3 ±2%	6.79 ±0.01
High Exposure Greywater Reuse (NSW Government, 2008)	<10	-	-	6.5-8.5

Removal efficiencies were calculated using the equation below:

$$Removal\ Efficiency\ \% = \frac{Influent\ Concentration - Effluent\ Concentration}{Initial\ Concentration} \times 100$$

Removal efficiencies for TSS, TDS and EC at different retention times are presented in Figure 10.

Visually it can be seen from Figure 8 that the effluent has become significantly clearer as a result of the filtration system. In terms of reducing turbidity, the system was successful. Though, this observation would have been more relevant with a quantifiable turbidity test. An attempt was made to conduct a simple low cost turbidity test. Outlined in (Myre & Shaw, 2006), this was done by placing a figure at the end of a clear glass tube. The tube was then filled with the liquid sample until the symbol was "barely visible". A conversion of the liquid height can then be made to produce a turbidity reading. However, after conducting this experiment it became apparent that this method was simply too inaccurate due to the subjectivity of readings, thus, this method was abandoned as the results would simply be too inaccurate. In the future it is recommended that turbidity readings be identified with a turbidity meter, allowing comparisons to grey water reuse requirements.

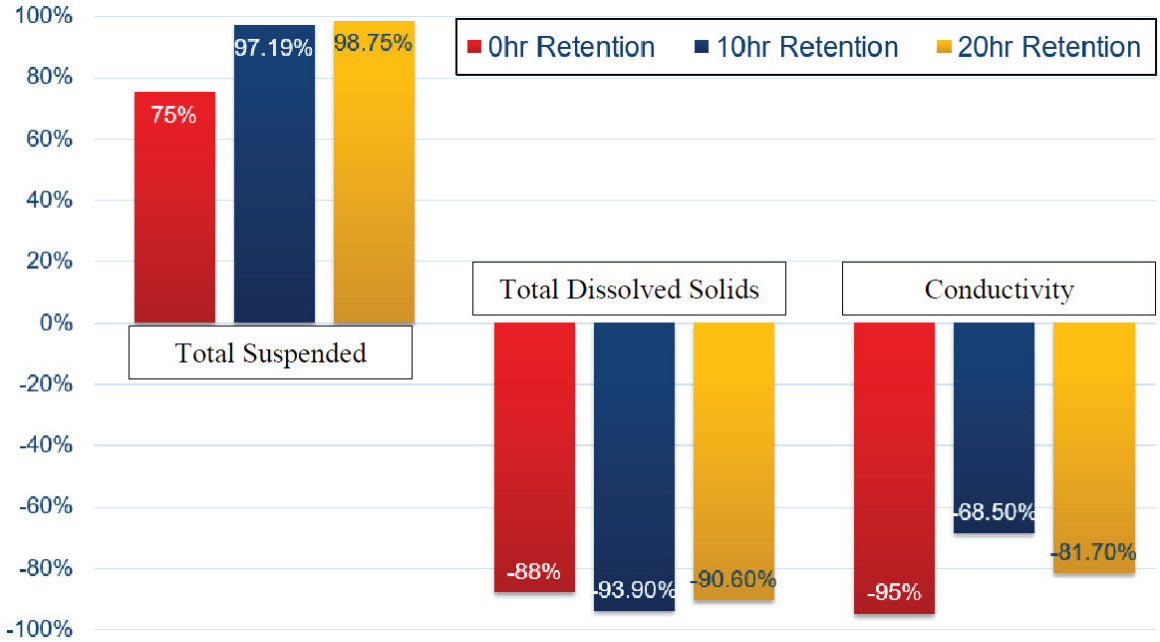

Figure 7 Removal Efficiencies

Discussion of Results

Results in Table 2 indicate that TSS of 10 and 20-hour retention times comfortably satisfy NSW government greywater reuse standards. Coupled with the increasing removal efficiencies of TSS for increasing retention times, the results indicate that retention time does play a large role in suspended solids removal. Visually this can be seen from samples in Figure 5. However, the experiment for 10 and 20-hour retention times were conducted 3-4 days after the no retention experiment. An increase of biological layer (Schmutzdecke) growth in the plant box and sand containers could partly account for the increases in TSS removal efficiencies. Although, it is doubtful that an increase in removal efficiency this large would occur at only 3-4 days apart. The addition of influent into the first plant container will undoubtable cause turbulence within the sand:soil:compost medium. In the no retention time experiment, however, this stirring effect could be more pronounced due to the rapid discharge rate. On the other hand, in the retained experiments, the medium has time to settle before being discharged. This stirring effect could account for the higher total suspended solids concentrations in the effluent. Intuitively then, the concentrations of dissolved solids should similarly be highest in the non-retained effluent. However, this is contradicted as there seems to be no correlation between retention time and dissolved solids removal efficiencies. A control experiment, replacing the plant container with a sand container should be conducted to compare if retention in the plant container actually plays a large role in solids removal. Although, a soil medium is still recommended as constructed wetland experiments by (Thurston, et al., 1996) revealed that soil systems outperformed pond systems in terms of total coliform, faecal coliform and coliphage (virus) removal efficiencies.

The levels of total dissolved solids (TDS) and electrical conductivity (EC) were extremely high compared to the levels found in spring and rainwater. Shown in Figure 7 the filtration system actually increased levels of TDS and EC significantly. Thus, the system was not successful in removing dissolved solids and minerals. An increase in TDS has been seen in some constructed wetland systems (Haddad, et al., 2012), and an increase in EC has been seen in sand filtration systems (Assayed, et al., 2014). However, the increases were not of a magnitude as large as seen in this experiment. Fine particles from the soil and compost medium could have contributed to this increase. Additionally, a soil-like odour was also observed in the effluent straight after the filtration system. Investigation could be taken to replace plant container with sand to identify the effects of soil and compost on TDS and EC. However, indicators for dissolved solids and conductivity are not required by NSW greywater reuse standards (NSW Government, 2008). And so, although these indicators illustrate a better picture of the water quality, they can be considered irrelevant for our intended use. pH levels in all experiments were found to be within greywater reuse standards. Interestingly, an increase in retention time produced pH levels closer to neutral 7 and levels found in spring and rainwater.

The experiments were conducted in sequence from no retention time to 20-hour retention time, with influent and effluent sample being collected at the end of each experiment. The sample were stored in clear plastic containers at ambient temperature. However, experiments to identify water characteristics were conducted after all experiment have been run, 7 days after the first experiment. And so, a long period between running the experiments and identifying water characteristics is expected to skew results. Microbial growth could occur in the container, especially as the samples were not stored in a cold controlled environment. Furthermore, influent indicators for TSS, TDS and EC were all higher in later experiments, and so higher influent concentrations in the latter experiments could offset the shorter effluent storage periods. Although it is unknown how much microbial levels would increase by in a 7-day period. In the future, the samples must be stored in a cold controlled environment or tested straight after the experiment to limit the effects of characteristic changes during storage.

Generally, characteristics in the synthetic greywater influent were similar to actual greywater taken from research, shown in Table 2. Total suspended solids, dissolved solids and pH were in the lower half of the range. Further research could be taken to conduct the experiments at higher concentrations to identify corresponding removal efficiencies. However, one of the main limitations of this experiment is the lack of biological indicators such as biological oxygen demand (BOD), E. coli levels as well as total coliform. High exposure greywater reuse guidelines require a number of biological requirements to be met. BOD <10mg/l, E. coli, coliphages (Virus) and clostridia (Bacteria) levels <1cfu/100ml (NSW Government, 2008). Cfu meaning colony-forming unit, a measurement of bacteria or fungal cells in a sample. To meet these requirement, it is vital that biological concentrations be observed. Although the system seems to be successful in removing suspended solids, the overall success was inconclusive due to the lack of imperative biological indicators.

Discussion of System and Construction

Terracotta was chosen due to its higher porosity compared to other conventional materials such as plastics. The higher porosity was expected to provide higher oxygen levels which provide better aerobic conditions for microbial breakdown. However, after working extensively with the terracotta pots it was evident that the material was not a very suitable. Drilling holes into the material became an unnecessarily arduous task even with the aid of water as a cooling liquid. Similarly, sealing the rubber tubes to the terracotta was extremely difficult due to the material's chalky surface. The substantial weigh of the material also became an issue as the whole system could not be mounted to the wall and was laborious to manoeuvre. In this way, although visually appealing, terracotta is not a recommended material to use as a filtration container. The discharge rate from each container was also observed to be quite rapid. This rapid discharge is expected to disturb the Schmutzdecke and agitate the sand:soil:compost medium, resulting is a lower removal efficiency. A more gradual discharge mechanism which requires less human involvement would be preferred. This could be in the form of a clay layer at the container's base which allow the liquid is gradually permeate out of the container. The system was at a reasonable price of $299. Apart from the terracotta pots, the second highest cost was from the activated carbon, accounting for 20% of total costs. The price for the premium grade carbon seems excessive and thus, selecting a lower grade activated carbon is recommended. The omission of terracotta containers and premium activated carbon present cost saving options. Although, the effects of using lower grade activated carbon on removal efficiencies should also be considered. The plants were implanted into the container only 1 month before experiments were conducted. However, (Kaseva, 2004) states the plant typically need a few mouths to be well established in a container. Further experiments could be conducted later on to identify removal efficiencies after ample root establishment.

Further variation to the experiment could be conducted to identify relationships between other variables and removal efficiencies. Recommendations include increasing the amount of plants, investigating longer retention times and allowing more time for plant root growth. These three factors are aimed at identifying the advantages and disadvantages of using plants in the filtration process. Moreover, after conducting all experiments, the plants were unearthed to identify the root matrix. Visually Phalris Arundinacea roots undoubtedly penetrated deeper and were denser than Oenathe Sarmentos (Water Parsley) roots. Solely judging from this observation, and the assumption that greater root penetration is better for the system, Phalris Arundinacea seems to be more appropriate over the Water Parsley. However, further investigation could be taken to compare removal efficiencies with plant roots mass, possibly through the measurement of dried root mass and treatment efficiency. Water losses were also not measured in this experiment. However, in the context of an off-grid housing unit conserving as much water as possible will become critical. Water losses could be even more critical when retention times increase significantly. (Kaseva, 2004) found 6.3-9.28% water losses while (Schütte & Fehr, 1992) found 20-50% summer evapotranspiration losses in the constructed wetland systems. Thus, it is recommended that an opaque membrane be used to cover the containers limiting the effects of evaporation. Further experiments could be taken to identify the rates of water loss in the system.

FURTHER WORK AND RECOMMENDATIONS

This project opens many possibilities to conduct further work into the area of greywater recycling. Due to time and space limitations many other experimental variations could not be produced within the time frame. As the project progressed, better experimental setups became apparent, and thus, this section will explore other experimental possibilities and recommendations for further work.Protruded Container System

Being part of a small off-grid housing unit, space is expected to always be quite limited. This was the main motivation of stacking the filtration boxes on top of one another. As seen in the experiment, placing pots on top of one another limits the ability to grow plants in every container. Unless vertical space is not a limiting factor, then sufficient space can be left between containers, however, this uses up a large amount of vertical space, resulting in a very tall system that is not desirable. A solution to this could be to produce plant container which individually have protruding compartments used to support plants. The compartment could protrude from the sides and front of the main container if need be. A systematic diagram of the design is presented in Figure 8 and Figure 9 below. If the container is made from clay, a section of the existing square box could be cut, and a protruding plant compartment moulded into the existing pot. Clay is the recommended method to produce these containers as it is readily available, cheap and is extremely workable. Placing the plants in the protruding containers will allow acceptance of sunlight even when the containers are stacked on top of each other. The benefits of the plant roots for filtration discussed in (Brix & Arias, 2005) and (Kadewa, et al., 2010) can be achieved as the roots are expected to grow into the main container absorbing nutrients.

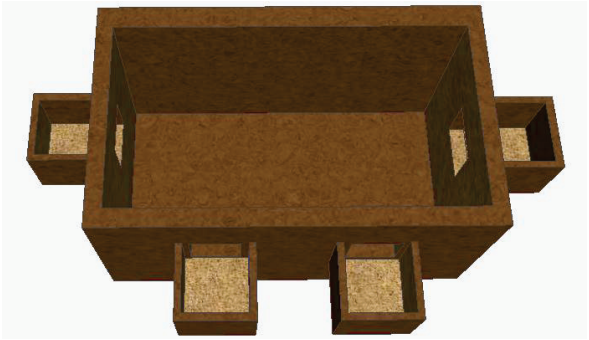

Figure 8 Extruding Box Individual Container Render

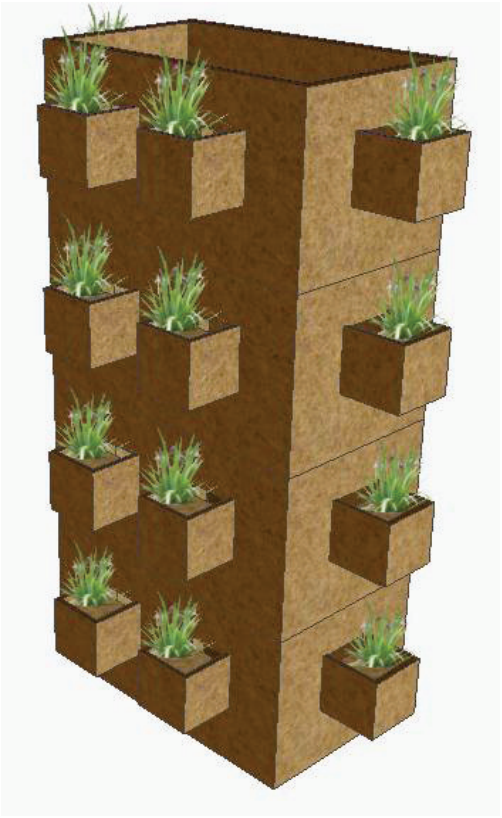

Figure 9 Extruding Container System Render

Hydroponic System

To successfully filter water using plants, the importance of retention time has become evident. This is to ensure there is sufficient time for the rhizosphere to interact with the influent. (Avery, et al., 2007) asserts that in practice, short circuiting (flood and flush) leads to variable retention times and poorer filtration performance. Thus, a system designed to have long retention times will reduce variability and improve performance. This is agreed by the experimental investigation as increasing retention time increased suspended solids removal. A system which influent is retained then flushed could be undesirable as there is still some degree of variability. A possibility could be to produce a system which has continuous, but extremely low hydraulic loading and drainage. This will ensure long retention times and maintain low variability within the system. A hydroponic system could be a solution to these requirements. Moreover, using hydroponics increases the growth rate of plants by 30-50% compared to soil plants under similar conditions (Haddad & Mizyed, 2011).

Loosely defined, a hydroponic system is when a plant is grown soilless, in a nutrient solution. There are two main hydroponic systems, solution culture, where the plant is loosely suspended over a nutrient solution, and medium culture, where the plant is held in place with an inactive soilless medium (Haddad & Mizyed, 2011). Although the disadvantage of using a hydroponics system is the longer filtration times needed compared to typical porous filters.

There are several researched hydroponic systems that have been successful in treating domestic wastewater. However, many systems incorporate an aeration tank to increase dissolved oxygen (DO) levels, especially when DO fluctuates significantly in domestic wastewater (Ottoson, et al., 2005) (Norström, et al., 2004) (Haddad & Mizyed, 2011). Though, treating domestic greywater would require less comprehensive methods than wastewater. Little research has been conducted specifically on greywater recycling with hydroponics. Nonetheless, gravity fed hydroponic system from (Haddad, et al., 2012) presented a successful example of wastewater treatment through hydroponics.

CONCLUSION

The overall water balance will continue to play a large role in the feasibility of an off-grid housing unit. In this particular context, rainwater harvesting is currently the only viable water source. Through the use of appropriate component such as first flush diverters, virgin resin storage tanks and metal rooftops, the efficiency and quality of harvested rainwater can be maximized. However, it is evident that a portion of water must be recycled to create a positive water balance. In this way, greywater recycling will also be an integral component of a feasible off-grid housing unit. Comprising 70% of daily water use, greywater can be recycled through inexpensive biological filters, which require no external energy input. Out of many researched biological filtration systems, constructed wetlands exhibited much promise in terms of filtration efficiency, aesthetic appeal, as well as the possibility of a food source. Filtration capabilities in the experiment's multi-container plant, sand and carbon system displayed promising results. The biological system met NSW high exposure water reuse standards in total suspended solids and pH levels. Exceptional removal efficiency for suspended solids of 98.75% was achieved by retaining the influent for 20 hours in the plant container. Though the system increased dissolved solids and electrical conductivity by up to 93.9 and 95%, respectively. However, the need for biological indicators such as biological oxygen demands and total coliform are equally if not more important due to health risks. Thus, the system's success remains inconclusive as further research needs to be conducted into the system's biological removal efficiencies. The protruding plant container design and hydroponic systems could pose as viable alternatives to current treatment systems. Further research could be conducted to identify the removal efficiencies and costs of these systems. As fears towards the effects of climate change continue to grow, society will continue to seek methods and system that reduce our negative externalities to the environment. This trend towards sustainability will undoubtable lead to a greater need for sustainable living, and as identified, off-grid housing units pose as a possible solution.

REFERENCES

1. University of Nebraska–Lincoln, 2008. *Choosing a Clay or Plastic Pot for Plants.* [Online] Available at: http://lancaster.unl.edu/hort/articles/2002/typeofpots.shtml[Accessed 2 October 2016].
2. Abs.gov.au, 2010. *Measures of Australia's Progress,.* [Online] Available at: http://www.abs.gov.au/ausstats/abs@.nsf/Lookup/by%20Subject/1370.0~2010~Chapter~Water%20consumpti

on%20per%20person%20(6.3.3)
[Accessed 9 May 2016].
3. Assayed, A., Chenoweth, J. & Pedley, S., 2014. Drawer compacted sand filter: a new and innovative method for on-site grey water treatment. *Environmental technology,* 35(19), pp. 2435-2446.
4. Avery, L. et al., 2007. Constructed wetlands for grey water treatment. *Ecohydrology & Hydrobiology,* 7(4), pp. 191-200.
5. Brix, H. & Arias, C., 2005. The use of vertical flow constructed wetlands for on-site treatment of domestic wastewater: New Danish guidelines. *Ecological Engineering,* 25(5), pp. 491-500.
6. Campos, L., Su, M., Graham, N. & Smith, S., 2002. Biomass development in slow sand filters. *Water Research,* 36(18), pp. 4543-4551.
7. Gleick, P., 1996. Basic water requirements for human activities: Meeting basic needs. *Water international,* 21(2), pp. 83-92.
8. Haddad, M. & Mizyed, N., 2011. Evaluation of various hydroponic techniques as decentralised wastewater treatment and reuse systems. *International Journal of Environmental Studies,* 68(4), p. 461.
9. Haddad, M., Mizyed, N. & Masoud, M., 2012. Evaluation of gradual hydroponic system for decentralized wastewater treatment and reuse in rural areas of Palestine. *International Journal of Agricultural and Biological Engineering,* 5(4), p. 47.
10. Howard, G. & Bartram, J., 2003. *Domestic water quantity, service level and health,* Geneva: World Health Organization.
11. Kadewa, W. et al., 2010. Comparison of grey water treatment performance by a cascading sand filter and a constructed wetland. *International Association on Water Pollution Research,* 62(7), p. 1471.
12. Kaseva, M., 2004. Performance of a sub-surface flow constructed wetland in polishing pre-treated wastewater: a tropical case study. *Water Research,* 38(3), pp. 681-687.
13. Kus, B., Kandasamy, J., Vigneswaran, S. & Shon, H., 2010. Analysis of first flush to improve the water quality in rainwater tanks. *Water science and technology: AJournal of the International Association on Water Pollution Research,* 61(2), p. 421.
14. Lee, J., Bak, G. & Han, M., 2012. Quality of roof-harvested rainwater--comparison of different roofing materials. *Environmental pollution,* Volume 162, pp. 422-429.
15. Li, F., Wichmann, K. & Otterpohl, R., 2009. Review of the technological approaches for grey water treatment and reuses. *Science of the Total Environment,* 407(11), pp. 3439-3449.
16. Masi, F. et al., 2010. Treatment of segregated black/grey domestic wastewater using constructed wetlands in the Mediterranean basin. *Water Science and Technology,* Volume 61, p. 97–105.
17. Mendez, C. et al., 2011. The effect of roofing material on the quality of harvested rainwater. *Water Research,* 45(5), pp. 2049-2059.
18. Myre, E. & Shaw, R., 2006. *The turbidity tube: simple and accurate measurement of turbidity in the field. ,* s.l.: Michigan Technological University.
19. Nghiem, L., Oschmann, N. & Schäfer, A., 2006. Fouling in greywater recycling by direct ultrafiltration. *Desalination,* 187(1), pp. 283-290.
20. Norström, A., Larsdotter, K. G. L., La Cour Jansen, J. & Dalhammar, G., 2004. A small scale hydroponics wastewater treatment system under Swedish conditions. *Water Science and Technology,* 48(11-12), pp. 161-167.
21. Novak, C., Van Giesen, E. & DeBusk, K., 2014. *Designing rainwater harvesting systems: integrating rainwater into building systems.* Hoboken: John Wiley & Sons.
22. NSW Government, 2008. *Interim NSW Guidelines for Management of Private Recycled Water Schemes,* Sydney: Department of Water and Energy.
23. Ottoson, J., Norström, A., Dalhammar, G. & Skolan för bioteknologi (BIO), K., 2005. Removal of micro-organisms in a small- scale hydroponics wastewater treatment system. *Letters in Applied Microbiology,* 40(6), pp. 443-447.
24. Schütte, H. & Fehr, G., 1992. Neue Erkenntnisse zum Bau und Betrieb von Pflanzenkläranlagen. *Korresp Abwasser ,* 39(6), pp. 872-9.
25. Thurston, J. et al., 1996. *Fate of indicator microorganisms, Giadia, and Cryptosporidium in two constructed wetlands.* Vienna, s.n.
26. VEWIN, 2006. *Vereniging van Waterbedrijven in Nederland,* Rijswijk: Waterleidingstatistiek.
27. WHO/UNICEF, 2000. *Global Water Supply and Sanitation Assessment,* Washington: WHO/UNICEF.

Retrofitted Green Roofs and Walls and Improvements in Thermal Comfort

Renato Castiglia Feitosa [1, a)] and Sara Wilkinson [2, b)]

[1] *Researcher at Oswaldo Cruz Foundation (Fiocruz), Department of Sanitation and Environmental Health of National School of Public Health, Brazil.*
[2]*School of Built Environment, Faculty of Design Architecture and Building UTS, Australia*.

[a)]Corresponding author: rentcf@yahoo.com.br
[b)]sara.wilkinson@uts.edu.au

Abstract. Increased urbanization has led to a worsening in the quality of life for many people living in large cities in respect of the urban heat island effect and increases of indoor temperatures in housing and other buildings. A solution may be to retrofit existing environments to their former conditions, with a combination of green infrastructures applied to existing walls and rooftops. Retrofitted green roofs may attenuate housing temperature. However, with tall buildings, facade areas are much larger compared to rooftop areas, the role of green walls in mitigating extreme temperatures is more pronounced. Thus, the combination of green roofs and green walls is expected to promote a better thermal performance in the building envelope. For this purpose, a modular vegetated system is adopted for covering both walls and rooftops. Rather than temperature itself, the heat index, which comprises the combined effect of temperature and relative humidity is used in the evaluation of thermal comfort in small scale experiments performed in Sydney - Australia, where identical timber framed structures prototypes (vegetated and non-vegetated) are compared. The results have shown a different understanding of thermal comfort improvement regarding heat index rather than temperature itself. The combination of green roof and walls has a valid role to play in heat index attenuation.

INTRODUCTION

High density population areas have led to a worsening in the quality of life for many people in large cities in respect of the urban heat island effect and increases of indoor temperatures in residential and other buildings. To worsen the present scenario, the total urban population is said to increase to 66% of world population or 6.3 billion people by 2050 [1]. This is also coupled with overall global temperature increases occurring as a result of global warming and climate change [2]. Consequently, as a result of population and temperature increases, there a potential trend for health issues related to heat stress especially in elderly populations [3, 4].

Retrofitting existing buildings may contribute as a partial solution to these problems through a combination of green roof and green walls applied to existing rooftops and walls, respectively. As presented by Wilkinson and Castiglia Feitosa [5] green roofs may attenuate housing temperature. However it is important to highlight that due to the common tall characteristics of buildings, facade areas are substantially larger than those from rooftops. Thus, it is expected a more pronounced effect of green walls in attenuating housing temperatures [6]. However the combination of green roof and green walls is likely to provide a better thermal performance in the building envelope. In this way the present work intended to investigate to what extent this was the case. With this goal, a modular vegetated system is adopted for covering both rooftops and walls.

Rather than temperature itself, the heat index that encompasses the simultaneous effect of relative humidity and temperature, is used as the indicator of thermal comfort in Sydney – Australia using small scale experiments that compares two identical timber framed structure prototypes where one is fully covered with vegetation (walls and rooftop), and the other is not.

Several countries are expected to be effected heat waves in the upcoming years due to climate change impacts. In addition, according to Mertz et al. [7] many developing countries are predicted to be affected by increased temperatures. Thus, retrofitting existing buildings in a short time frame may comprise a suitable and viable solution.

Off-Grid Technology Workshop
AIP Conf. Proc. 1856, 020006-1–020006-8; doi: 10.1063/1.4985558
Published by AIP Publishing. 978-0-7354-1530-0/$30.00

The present research sought to evaluate the thermal performance of lightweight and low cost systems in retrofitting green walls and rooftops from existing buildings with no need of structural reinforcement. It also sets out the rationale for research design and experimental setups. The results presented show the performance of the vegetated structure in heat index attenuation, when compared to the non-vegetated structure.

METHODS

The methodology adopted herein encompasses the use of adaptive techniques that aim to mitigate the problems caused by increasing urbanisation, such as heat island effects and high internal housing temperatures promoted by direct solar radiation. A proposed solution for this issue is the use of lightweight vegetated modular systems that allow planting, cultivation and maintenance to be undertaken off site. This low cost technique is a simple and straightforward application for existing walls and rooftops. However, due to the significant and growing numbers of tall buildings in urban centres, facades become more relevant than rooftop areas in terms of heat exchange as they offer a greater area to plant out which is also highly visible to many people increasing the Biophilic effect [8].

Experimental Procedure

In order to evaluate the combined effect of green roofs and green walls an experimental setup was established at the University of Technology Sydney (UTS) Australia, using a selection of succulent plants due to their low risk of fire, drought resistance and good capability of development in shallow substrates that, in turn, avoided the need of structural reinforcement.

As shown in the Fig. 1 the adopted system comprise modular characteristics that make it possible to apply previously planted vegetated modules onto existing roof coverings, comprising either metal sheeting, roof tiles, or concrete roof slabs. To avoid the soil particles loss, it used a permeable fabric that separates the substrate from drainage and storage system that can retro feed the soil with water vapour during the evaporation process. Additional details about the methodology can be found in Wilkinson and Castiglia Feitosa [9].

FIGURE 1. Green roof and green walls experimental setup.

The green wall methodology was designed originally at Oswaldo Cruz Foundation (Fiocruz) Brazil is not presented in this paper, but is described by Wilkinson and Castiglia Feitosa [9]. In the experimental setup performed in Sydney plastic closed boxes, with six circular shaped openings drilled into the outer face in a three row and two column array, were used as containers for soil and plants. In this case, 5 cm of substrate is placed into the container

before being covered by geotextile fabric, and then sealed by the cover of the container box. Once this was completed, the plants were set in soil through small cuts in the geotextile fabric, and after the plants had established themselves, the boxes are placed by in "U" shaped metal profiles screw fixed to the external wall. The combined effect of vegetated roof and walls in heat index attenuation is performed by comparing two identical prototypes constructed with a 100mm thick timber framed structure covered with 13mm thick cement board, where one is fully covered with vegetation on walls and the roof, a profiled metal sheet covering, and the other structure is not (see Fig.1).

Heat Index Evaluation

Records of temperature and relative humidity were taken every 30 minutes, simultaneously inside the vegetated and non-vegetated prototypes by using data loggers supplied by Extech RHT10 over 92 days, from January 19th 2016 to April 20th 2016.

The heat index expresses the “apparent temperature” in degrees Celsius or Fahrenheit as a combined effect of relative humidity and air temperature. It is used by the National Weather Service (NWS), U.S. Government that provides weather forecasts and warnings of hazardous weather. Instead of considering only the influence of temperature on thermal comfort evaluation, the “apparent temperature” indicates the heat sensation due to the effect of relative humidity that indicates the amount of moisture in the air [10].

Relative humidity plays a relevant role on thermal comfort evaluation, once it is responsible for regulating the evaporation rate of sweat from the skin that responds to the cooling of the human body. Higher levels of relative humidity mitigate sweat evaporation from the skin, and increase the sensation of heat experienced by human beings [10].

In terms of environmental health research, the work carried by Steadman [11] provides the basis for the so called Steadman’s apparent temperature. It translates the combined effect of relative humidity and temperature into a scale called heat index that has the same units of temperature.

Anderson et al. [6] investigated and compared 21 algorithms that calculate heat index as a function of temperature and relative humidity, or dew point temperature. These authors pointed out that NWS algorithm [12], presented in the flowchart below (Fig.2), had the best fit Steadman’s table [11], and as a result it was chosen to calculate heat index in the present work. It is worth highlighting that initially heat index values were calculated using temperature unit measured in degrees Fahrenheit. These results were later converted to degrees Celsius.

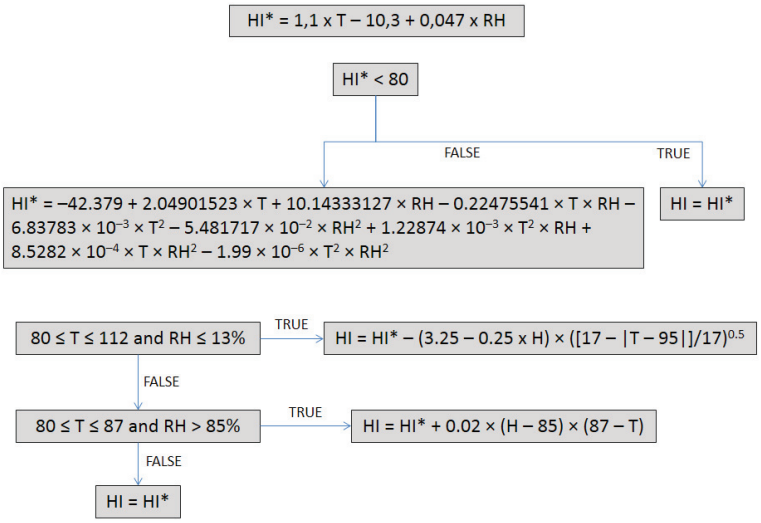

FIGURE 2. Flowchart of the algorithm of heat index (HI) calculation used by NWS based on air temperature in degrees Fahrenheit (T) and relative humidity in per cent (RH).

The risk analysis assessment in terms of heat stress is related to heat index according to the following heat advisory categories described in Table 1, which evaluates the likelihood of heat disorders with prolonged exposure or strenuous activity.

TABLE 1. Classification of heat advisories in United States according to NWS.

Categories	Heat Index	Possible Heat Disorders for People in High Risk Groups
Extreme danger	> 54°C	Heat stroke or sunstroke likely.
Danger	41 - 54°C	Sunstroke, muscle cramps, and/or heat exhaustion likely. Heatstroke possible with prolonged exposure and/or physical activity.
Extreme caution	32 - 41°C	Sunstroke, muscle cramps, and/or heat exhaustion possible with prolonged exposure and/or physical activity.
Caution	27 - 32°C	Fatigue possible with prolonged exposure and/or physical activity.

RESULTS AND DISCUSSION

Figure 3 presents a comparison between relative humidity, temperature, and the calculated heat index according to the NSW algorithm, during a 92 day-period that comprised mostly summer and mid-autumn seasons in Sydney. In addition, Table 2 summarises the maximum, minimum and average of the measured parameters, relative humidity and temperature, and their associated values of heat index for both non-vegetated and vegetated structures.

TABLE 2. Sydney maximum, minimum and average limits of temperature, relative humidity and heat index.

Categories	Temperature		Relative Humidity		Heat Index	
	Vegetated	Non-vegetated	Vegetated	Non-vegetated	Vegetated	Non-vegetated
Maximum	33.0	42.0	88.5	81.3	36.3	55.9
Minimum	15.5	15.4	38.6	36.3	15.5	15.4
Average	23.4	24.8	74	65.5	23.6	25.6

All limits of relative humidity levels were higher for the vegetated structure, when compared to the non-vegetated one. It indicated an influx of moisture into the vegetated prototype due to evapotranspiration process of plants. In the Fig.3 it can be seen that the records of relative humidity in the vegetated structure were permanently higher than those from the non-vegetated structure.

The maximum temperatures were registered during the daytime, whereas the lowest occurred during early morning hours. When compared to temperature the higher levels of heat index were substantially higher. However, according to the algorithm used, the minimum values of heat index and temperature are about the same for temperatures lower than 26.7°C.

Based on the temperature attenuation, as depicted in Fig. 3 the temperature differences varied from -1.1°C to 12.0°C. The positive differences mean that the non-vegetated structure was warmer than the vegetated structure during the daytime, while the negative differences (vegetated structure warmer than non-vegetated structure) were commonly registered in the night-time and early morning.

In terms of heat index, the difference between the non-vegetated, and the vegetated structure varied from -3.4°C to 21°C. It can be highlighted that in terms of heat index the influence of vegetation is even more pronounced when comparing vegetated to non-vegetated structure. As a result it is evident an increase in the ranges of temperature attenuation. The temperature showed to be more effective on heat index. However, relative higher levels of relative humidity in vegetated structures may counteract the effects of attenuation of temperature promoted by the vegetation. In the present case besides the vegetated structure having higher relative humidity levels than non-vegetated structure, such levels were not substantial to offset the effects of relative humidity.

FIGURE 3. Comparisons between relative humidity, temperature, and calculated heat index

In the results presented, the efficiency in temperature and heat index attenuation is relevant. Table 3 presents a summary of the measured parameters of temperature and relative humidity, and their respective calculated values of heat index.

TABLE 3. Sydney maximum, minimum and average limits of temperature, relative humidity and heat index.

Parameters		Non-vegetated (NV)	Vegetated	Difference (NV) – (V)	Simultaneous Difference
Temperature	Maximum	42.0	33.0	9.0	12.0
	Minimum	15.4	15.5	-0.1	-1.1
	Average	24.8	23.4	1.4	-
Relative Humidity	Maximum	81.3	88.5	-7.2	21.8
	Minimum	36.3	38.6	-2.3	-3.4
	Average	65.5	74.0	-8.5	-
Heat Index	Maximum	55.9	36.3	19.6	28.1
	Minimum	15.4	15.5	-0.1	-5.5
	Average	25.6	23.6	2.0	-

Compared to the previous work undertaken by Wilkinson and Castiglia Feitosa [9] that considered only the influence of vegetated roofs in attenuation of internal temperature in metallic sheds, a new set of experiments using different building materials was carried out to evaluate the simultaneous of vegetated walls and roof.

Comparing the both timber-framed structures, the experiments showed significant differences between the non-vegetated and the vegetated prototypes. The dark blue colour used on the walls of the prototypes, increased the internal temperature differences to a greater extent, due to the contrast of the surface temperatures between the uncovered walls and shaded walls by vegetation

The evaluation of thermal comfort is not only influenced by temperature but also by relative humidity levels. Compared to non-vegetated structure, it was observed that higher levels of relative humidity prevailed in the vegetated structure, even under lower temperatures. This fact indicates the moisture influx due to vegetation transpiration into the vegetated structure. Based on the combined influence of temperature and relative humidity in determining heat index, the additional moisture supply increases the relative humidity in the vegetated structure, offsetting the temperature attenuation promoted by the vegetation.

The addition of vegetation to walls and roof increase the thermal performance quantified by the U-value parameter that indicates the amount of heat transferred through a surface. Low U-values indicate good levels of thermal insulation, whereas high U-values indicate the opposite. Wong et al [13] identified in a originally non-thermal insulating building a reduction in U-value from 2.39 to 1.19 W/m²K after its roof covered with turf. In addition, Alcazar & Bass [14] and Castleton [15] also evidenced the role of vegetation in reducing U-value. According to Castleton [15] the addition of vegetation to walls and roofs increases not only insulation, but also thermal mass that comprises the materials potential to retain energy, and thus, provide inertia against temperature fluctuations. As a result, in the vegetated structure there is a temperature peak delay when compared to the non-vegetated structure.

The heat stress evaluation is shown according the histogram in Fig. 4 that compares the heat index of the vegetated and the non-vegetated structures over 92 days, according to the percentage of time that their values lie on the heat advisory categories shown in table 1.

According to Fig. 4 the adoption of combined systems of vegetated walls and roofs reduced the percentage of time under conditions from caution to danger in about 19% of cases. In terms of extreme heat conditions, the extreme caution episodes were reduced from 7.6% to 0.4% and the danger conditions from 4.1% to 0%.

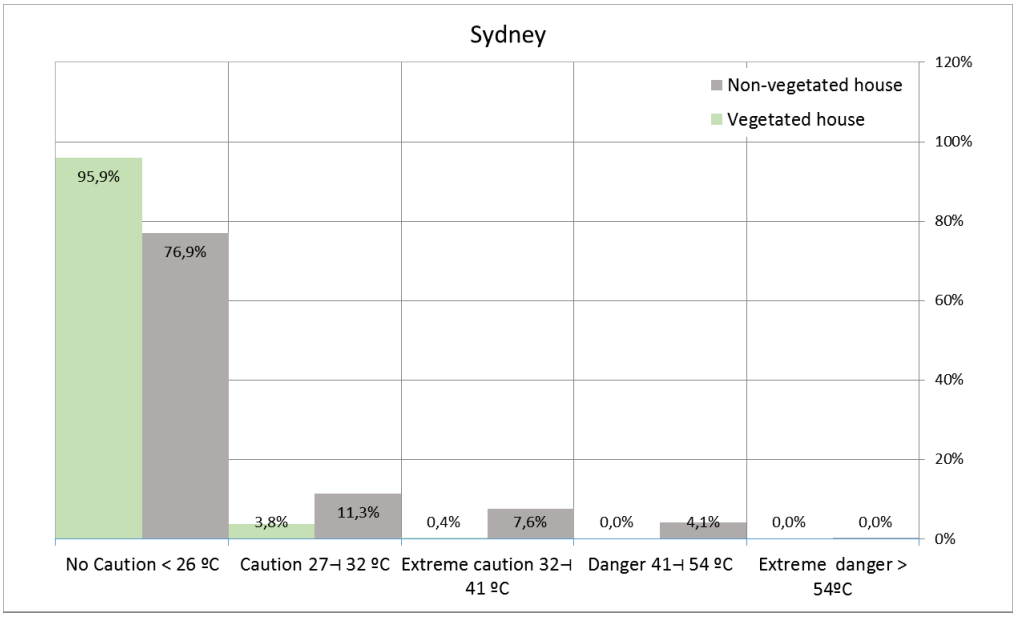

FIGURE 4. Comparison between Non-vegetated and vegetated houses in relation to percentage of time, along 92 days according to the Classification of heat advisories in United States - NWS (2016).

CONCLUSIONS

The modular system used in the experimental setup has shown good potential in heat index attenuation. However, in tall buildings it is important to note that the cooling effect of vegetated roofs will only extend to few floors below the roof. Thus, in terms of improving general thermal comfort it is important to consider the addition of vegetation to building facades.

The temperature attenuation observed was significant when comparing vegetated to non-vegetated structures. It is important to highlight that the dark blue colour used on prototype's walls increased the temperature differences observed more due to heat absorption by dark surfaces of the non-vegetated structure in contrast to shaded walls by the vegetated structure.

The relative humidity levels of the vegetated structure was higher along almost all of the data set indicating that the moisture influx into vegetated structure is due to transpiration of the plants.

The heat index depends on the simultaneous combination of temperature and relative humidity in order to assess the role of vegetated surfaces in thermal comfort promotion. So, the eventual moisture influx due to the plants' transpiration into the vegetated structure can offset the temperature attenuation observed, and increases the heat index values.

It is important to consider that moisture influx may also be attributed to experimental particularities, such as small openings between the roof and walls and also due to walls' porosity. It is expected that the use of coatings will increase the impervious properties of the walls, as well as a sealing the joint between the roof covering and the walls, will prevent any moisture ingress into the structure. Although the experimental scale of the experimental setup presented here is modest, it is important to take into account the combined effect of the vegetated roof and walls in heat index attenuation. Moreover, it is expected that vegetated walls can contribute integrally as a cooling mechanism, especially in floors of buildings where there is no contact with roof top areas

With regards to thermal comfort assessment, the classification of heat advisories is based on heat index limits which are categorized to evaluate the risk of possible heat disorders for people in high risk groups. According to observations presented in the results, the combination of the vegetated walls and roofs reduced the percentage of time under conditions from caution to danger by approximately 19%. Extreme heat conditions, extreme caution and danger episodes were reduced correspondingly from 7.6% to 0.4% and from 4.1% to 0%, respectively.

The combination of the vegetated walls and roof is shown to have a significant influence in promoting thermal comfort, keeping buildings in good health without the use of air conditioning systems, which, in turn, can lead to substantial energy savings. Thus, it is important to bear in mind that the use of off grid technologies not only

improves welfare conditions, but also has indirect effects that can improve environmental conditions and lower the demand for energy generation for cooling environments.

REFERENCES

1. RICS Futures: Our Changing World. Accessed on 13th August 2016 from www.rics.org (2016)
2. Intergovernmental Panel on Climate Change, Climate Change - Impacts, Adaptation and Vulnerability: Regional Aspects. Cambridge University Press (2014).
3. R Basu,. and J. M.Samet, "Relation between elevated ambient temperature and mortality: a review of the epidemiologic evidence", Epidemiologic reviews, **24**), 190-202 (2002).
4. G. Luber, and M. McGeehin,, "Climate change and extreme heat events", American journal of preventive medicine **35**, 429-435 (2008).
5. S. J. Wilkinson and R. Castiglia Feitosa, "Thermal Performance In Green Roof Retrofit," in *Green Roof Retrofit: building urban resilience*, edited by S. J. Wilkinson and T. Dixon (Wiley-Blackwell, London, 2016), pp. 62–84.
6. K. Perini, M. Ottelé, A. L .A. Fraaij, E. M. Haas, R. Raiteri, "Vertical greening systems and the effect on air flow and temperature on the building envelope", Building and Environment, **46**, 2287-2294 (2011).
7. O. Mertz, K. Halsnaes, J. E. Olesen and K. Rasmussen, "Adaptation to climate change in developing countries", Environmental management **45**, 743–752 (2009).
8. M. Ignatieva, and K. Ahrné, "Biodiverse green infrastructure for the 21st century: from "green desert" of lawns to biophilic cities", Journal of Architecture and Urbanism, **37**, 1-9 (2013).
9. S. J. Wilkinson and R. Castiglia Feitosa, "Retrofitting Housing with Lightweight Green Roof Technology in Sydney, Australia, and Rio de Janeiro, Brazil", Sustainability **7**, 1081–1098 (2015).
10. G. B. Anderson, M. L. Bell, R.D. Peng, "Methods to calculate the heat index as an exposure metric in environmental health research', Environmental Health Perspectives", Environmental Health Perspectives **10**, 1111–1119 (2013).
11. R. G. Steadman, "The assessment of sultriness. Part I: A temperature-humidity index based on human physiology and clothing science", Journal Applied Meteorology **18**, 861–873 (1979).
12. NWS (National Weather Service), Meteorological Conversions and Calculations: Heat Index Calculator. Available: http://www.hpc.ncep.noaa.gov/html/heatindex. html [accessed 10 December 2016].
13. N. H. Wong, D. K. W. Cheong, H. Yan, J. Soh, C.L. Ong, A. Sia, "The effects of rooftop garden on energy consumption of a commercial building in Singapore", Energy and Buildings **35**, 353–364 (2003).
14. S. Alcazar, B. Bass "Energy performance of green roofs in a multi storey residential building in Madrid", in *Greening Rooftops for Sustainable Communities; Green Roofs for Healthy Cities*, Washington, DC, USA, (2005)
15. H. Castleton, "Green roofs: building energy savings and the potential for retrofit", Energy and Buildings **42**, 1582–1591 (2010).

Stand Alone Solar Energy Harvesting and Storage Systems in Off-Grid Applications

Fernando Alonso-Marroquin[1,a)], Justin Blake Gormly[1)], and Jose Bilbao[2)]

[1]*School of Civil Engineering, University of Sydney, NSW 201, Australia*
[2]*Systems Group, School of Photovoltaic and Renewable Energy Engineering, The University of New South Wales, Australia*

[a)]Corresponding author: fernando@sydney.edu.au

Abstract. The following is an implementation of a stand-alone system for solar energy harvesting and electrical energy storage systems for use in off-grid housing applications. The principal aim of this project was to construct a compact and affordable system for an off-grid house and to monitor its efficiency along the year.

INTRODUCTION

The essential concept of an off-grid system is to attempt to separate the dependence of a shelter's primary living systems from public infrastructure and utilities.

Many lifestyles and applications require off-grid systems due to their lack of proximity to an energy grid of any kind. These include remote settlements, inland farms, marine vessels, stationary oil rigs, remote telecommunication systems, alpine and desert postings, and many others. In addition to off-grid energy systems built from necessity, a growing trend of voluntary off-grid living is present in the global market. The continuous reduction of price in solar panels and batteries had led to a growing tendency of living off the grid [1].

Aside from the specialized applications described and the trends in the market, the greatest proportion of the global population with no connection to grid utilities are those who due to poverty and lack of infrastructure are unable to access electricity, water and waste systems. According to the World Bank 15.4% of the global population were lacking access to electricity in 2012 [2]. In addition to impoverished areas, the instance of natural disasters has the potential to incapacitate public utility grids and networks, which creates the necessity of temporary off-grid systems.

This project will examine the possibilities of an off-grid solar energy system, also called stand-alone solar system, in an urban area in Sydney, Australia. This will include the setup of a solar energy system using commercially available components and analysis of performance under sunny and cloudy conditions in the Sydney region.

Off-Grid Technology Workshop
AIP Conf. Proc. 1856, 020007-1–020007-6; doi: 10.1063/1.4985559
Published by AIP Publishing. 978-0-7354-1530-0/$30.00

SYSTEM COMPONENTS

The system was installed as shown in Figure 1. Two solar panels of 180 W at standard test conditions (STC) are connected in parallel to the charge controller. The battery and inverter are then wired into their respective input terminals on the charge controller. The system was design to work with standard extra low voltage (ELV) components (12V) and all wiring was completed using a dual core copper wire selected accordingly.

The multimeters used for data-logging were installed as follows; the amperage meter was connected in series on the positive connector of the solar array, and the voltage meter was connected in parallel on the solar array input terminals through a 20 m wire extension. These multimeters were then connected to a 9 V DC power source to allow them to have an indefinite supply of power for long-term data logging. Each multimeter was then synced to a separate PC computer via a Wi-Fi module for connection and interface with the data logging software.

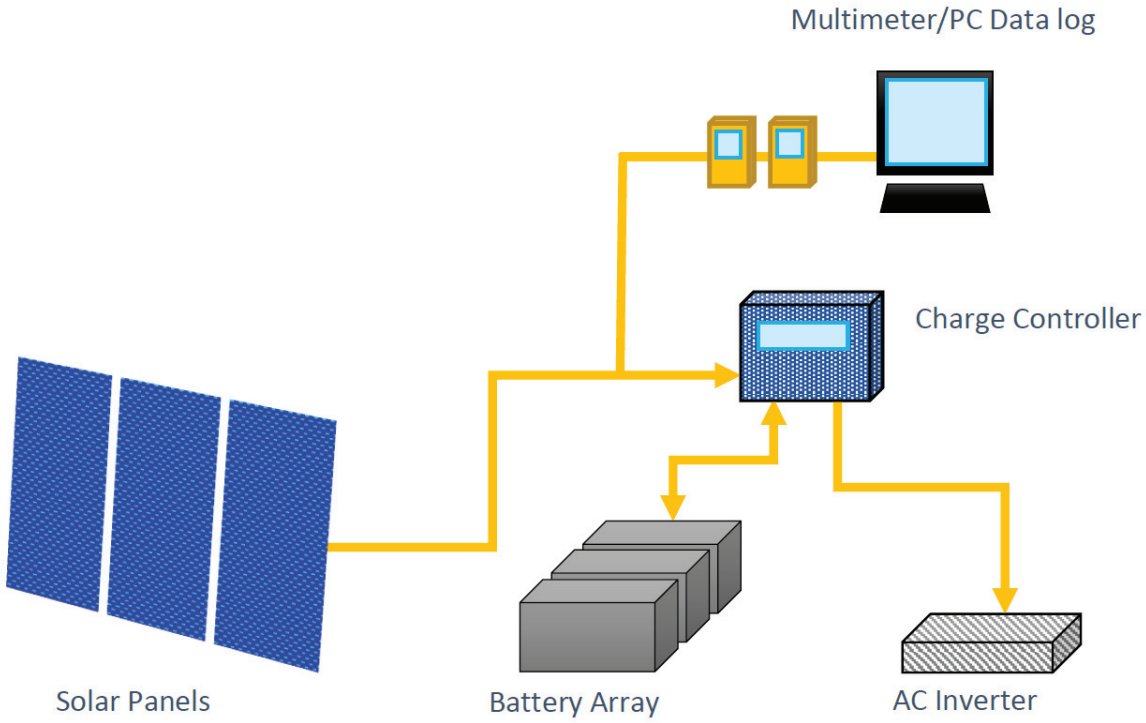

Figure 1: Diagram of the solar system and data logging equipment

Solar Panels

The panels chosen for the system were two 180W Powertech flexible silicone monocrystalline panels, see Figure 2. The efficiency of the panel is calculated using the formula

Efficiency = Power of solar panel/ (area of solar panel × nominal solar power)

The dimensions of the panels are 1.3m × 0.8m and had a nominal voltage of 12V with a maximum power voltage (P_{MAX}) of 180W. The nominal solar power is 1000W/m^2. Thus the efficiency is 13.3%.

The full specifications of the panels including the voltage and intensity at maximal power (MP) V_{MP} and I_{MP} are displayed in Figure 3 below

Figure 2: Uninstalled solar panels undergoing preliminary tests

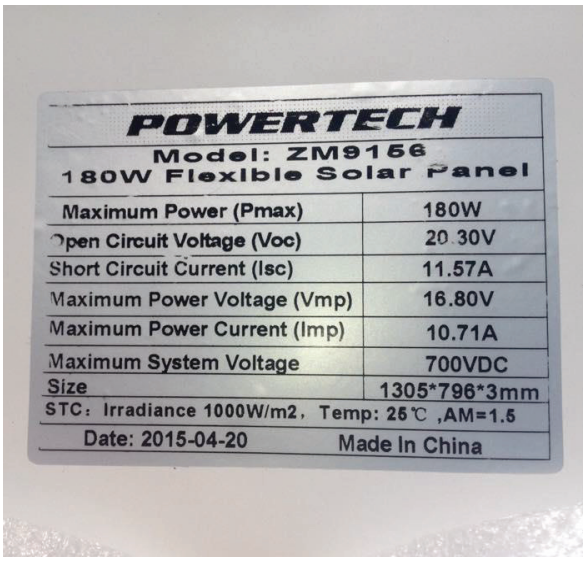

Figure 3: Full manufacturer's performance specifications of solar panels

Battery

For the system, we installed a single 12 V, 100 Ah deep cycle gel sealed acid battery, see Figure 4. The 100 Ah (amp-hour) refers to the capacity at a 10 Amperes draw in 10 hours. Multiplying this value by the voltage of the battery gives the capacity in watt hours at this amperage draw. As such, the capacity is

Total energy = 12 V ×100 Ah = 1200 Wh = 1.2 kWh

A simple battery test was implemented with the aim of gaining a practical measure of the battery's capacity based on its performance when connected to the entire system. A simulated appliance load of 10.9 amps (exerted by two halogen lights and a submersible water pump) was placed on the system without any assistance from the solar panels. The time taken to drain the battery was recorded which came out at an average of 9.24 ± 0.2 hours based on 3 tests. If we multiply the hours by the 10.9 A load one can retrieve a figure for the battery capacity of 100.72Ah. The test are consistent with the specified discharged times specified in the product, which are included in Table 1.

Discharging time	Capacity	Energy
1 hour	58.5 Ah	0.702 kWh
5 hours	81 Ah	0.972 kWh
10 hours	100 Ah	1.2 kWh
20 hours	102 Ah	1.224 kWh

Table 1: Specification of capacity of the battery versus discharging time

Solar controller

The solar controller in Figure 5 is a programmable Powertech controller. The controller operates either at 12 V or 24 V inputs from the solar panels and from the batteries, but it has a 12V output. The controller has a maximum current draw on the batteries of 30 amps and an efficiency rating of 97%.

Inverter

The inverter selected was a Powertec 12 V pure sinewave inverter, shown in Figure 6. . It has an 1100 W continuous power capacity and a 2200 W surge capacity. For 240 V appliances (as is the AC output voltage for the inverter), the inverter has a maximum continuous current draw of 4.58 amps. The manufacturer gives an averaged efficiency rating of 90% for this unit.

Figure 4: Deep cycle battery chosen for the system

Figure 5: 30A Powertech solar controller

Figure 6: 1100W 12V inverter installed in energy system.

OFF-GRID UNIT

The site provided for the off-grid house was on the grounds of The University of Sydney's campus. The main structures of the house are primarily comprised of timber, with poured concrete footing foundations and a corrugated iron roof. The footprint of the building measures approximately 2 m × 3 m and has a height from the finished floor level to the interior ceiling of approximately 2.4 m. In addition to this, the entire house is raised 0.8 m off the ground on 100 mm × 100 mm square timber posts. A photo of the building in its current state at the time of writing this report is shown in Figure 7 below.

To mount the solar panels to the roof, a frame was constructed from a galvanized steel rail extrusion bolted onto two 20 mm × 20 mm steel square hollow sections. The purpose of this was to raise the panels off the surface of the roof so as to allow an adequate airflow between the two surfaces, thereby minimizing the temperature of the panels.

The solar panels were wired together in parallel through connecting the output terminal connectors with a set of y-harnesses so as to have positive to positive terminal and negative to negative terminal. This was done in order to keep the nominal voltage of all components of the system at 12 V for simplicity. A 10 m dual core wire designed for 12 V DC applications was then connected to the outgoing terminals for the pair of panels which could then be wired to the controller. A 16 A DC circuit breaker switch was also wired in to this circuit so as to be able to cut the power from the solar panels. The battery, inverter, and solar controller were stored inside the house. Each component of the system, including the panels, were wired together with the same 12 V cable as used for the outgoing cable of the solar panels.

To monitor the energy input from the solar panels over the course of the day, two identical digital multimeters were installed into the system, each of which having a wireless PC interface via a Wi-Fi connection module. This allowed for continuous logging of data values from the multimeters at selectable time interval. The multimeters are Digitech IP67 qm 1571. The accuracies for DC voltage measurement are ±0.5% and DC amp measurement ±1.4%.

Both multimeters were wired onto the solar panel input wires at the charge controller, the first being connected in series with the positive cable so as to measure the amperage and the second being connected in parallel with the positive and negative ports on the controller. Initially, the intention was to have a single computer inside the house to log the incoming data from both multimeters, however it was found that signal interference between the two multimeters led to unreliable data collection, with values coming in at irregular time intervals. To overcome this, a second computer was set up in an adjacent building and a 20 m cable was wired in parallel to the solar panel ports on the charge controller so as to be able to relocate the second multimeter out of range of the first.

Figure 7: Mounting frame detail and mounting position of the solar panels on the roof.

RESULTS

In analyzing the data from the multimeters, plots of the each of the data sets with respect to time were produced, so to generate statistics for total solar energy collection over the course of a day. The method of calculating total energy was to take the product of the voltage and the amperage logs to produce a plot of the power output in watts. This power plot is then integrated over the 24 hour interval where measurements took place, so as to retrieve a figure for the total energy collected in watt-hours or kilowatt-hours. The plots on the following pages are representative of a typical data set. The most important parameter is that of the total energy collected in kilowatt-hours, calculated as the integral of the function of power output (voltage times intensity) with respect to time over the given 24 hour interval.

Test conditions

Meteorological conditions significant affect energy collection potential. Hence, the system was tested under various weather conditions such as a sunny day, a day with moderate cloud cover, and a day with heavy cloud cover. The following data set is from the 24th of October, which had the most hours of sunlight for entire month at 12.4 h according to the Bureau of Meteorology; 22nd of October, which had significant cloud cover throughout the day; and 20th of October, which was observed to have moderate cloud cover. The values of power versus time are included in the Figure 8 and the total energy collected in these three cases are included in Table 2.

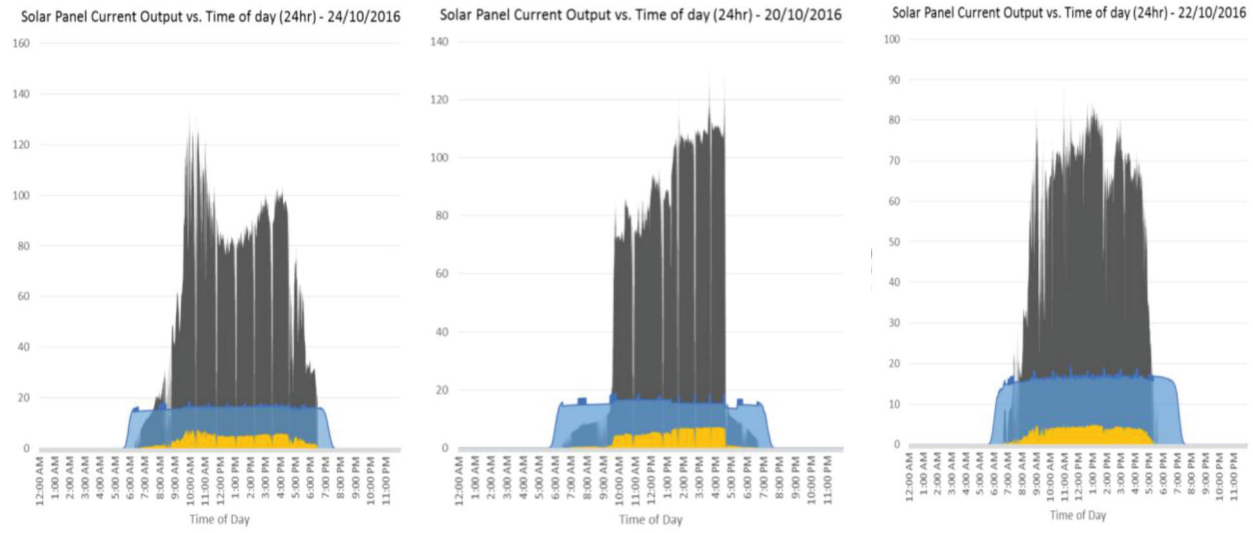

(a) (b) (c)

Figure 8: Solar energy data set – (a) 24th October 2016 (Sunny/clear conditions), (b) 20th October 2016 (rainy conditions), (c) 22th October 2016 (moderate cloud conditions), Power (black) is given in Watts, and it is calculated as the product of voltage (blue) and intensity (yellow). The voltage remains approximated constant around 15 Volts (scale not shown).

Maximal values	Sunny day	Moderate day	Rainy day
Amperage (A)	7.96	7.43	5.42
Voltage (V)	18.61	18.9	19.66
Power (W)	139.21	129.90	90.73
Total Energy Collected (kWh)	0.785	0.673	0.610

Table 2: Summary of the harvested energy data

CONCLUSIONS

In analyzing the results of the solar energy collection tests, the main point of contact for comparison is the 1.2kWh energy that can be collected from the battery in 10 hours. On a day where the panels performed at their best, the total energy collection was 0.785 kWh. This equates to 65.4% of the storage capacity of the battery.

REFERENCES

1. Khalilpour R, Vassallo A. Leaving the grid: An ambition or a real choice? Energy Policy. 2015 Jul 31;82:207-21.
2. World Bank 2015, Improved Water Source Rural (% of rural population with access), viewed 25/04/16 - 13/05/16 http://beta.data.worldbank.org/indicator/SH.H2O.SAFE.RU.ZS